International Journal of Pharmaceutics 590 (2020) 119931

Contents lists available at ScienceDirect

International Journal of Pharmaceutics

journal homepage: www.elsevier.com/locate/ijpharm

Simulation of pellet coating in Wurster coaters

Hamid Reza Norouzi

Center of Engineering and Multiscale Modeling of Fluid Flow (CEMF), Department of Chemical Engineering, Amirkabir University of Technology (Tehran Polytechnique), PO Box: 15875-4413, Hafez 424, Tehran, Iran

ARTICLE INFO

Keywords:
Wurster coater
Discrete droplet method
Inter-particle variability
Circulation time
CFD-DEM

ABSTRACT

A combination of computational fluid dynamics (CFD), discrete element method (DEM), and discrete droplet method (DDM), i.e., a CFD-DEM-DDM model, was developed to simulate coating of pellets in a Wurster coater. The model equations were implemented in parallel using an approach that uses the computational resources of both CPU and GPU. Effects of the gas flow pattern, inlet gas temperature, partition gap, and spray characteristics were studied on the process. Decreasing the peripheral gas velocity, increasing the central jet velocity, and reducing the partition gap caused more uniform distributions of the circulation time and draft tube time, while the inlet gas temperature had negligible effect on them. Very high jet velocity caused a wider distribution of the circulation time. The dynamics of the spray and its interaction with pellets had significant effects on the coating mass distribution. Widening the spray angle while maintaining the droplet size constant caused the most uniform coating mass distribution and the highest deposition rate. Heat and mass transfer conditions as well as the deposition pattern changed the distributions of the solvent content and temperature of the pellets.

1. Introduction

Tablets and pellets are common formulations of pharmaceutical products. They are usually coated with one or multiple layers of films to cover the unpleasant odor of medicines, improve their appearance; and give them enteric, delayed (Shah et al., 2017) and/or sustained release (Kaur et al., 2020) properties. Large particles are usually coated in rotating drums (Ban et al., 2017; Boehling et al., 2016) or similar apparatus, while smaller particles and powders are coated in gas–solid contactors like fluidized beds and Wurster coaters (Hampel et al., 2012; Turton et al., 1998). In the Wurster coater, coating solution is introduced (as the film coating agent) into the bed through a bottom spray. Pellets are regularly directed into a central draft tube at the bottom, where the sprayed solution and the pellets come into contact. The holes on the distributor plate are configured in a way that hot gas (air or nitrogen) enters into the bed with a special pattern. The hot gas provides enough energy to vaporize the solvent of the coating solution (Christensen and Bertelsen, 1997; Teunou and Poncelet, 2002).

The design of the Wurster coater should provide conditions in which it uniformly distributes the coating solution on the pellets, eliminates agglomeration by providing good contact between the pellets and the hot gas, and limits pellet temperature to prevent APIs from being damaged. Inter-particle and intra-particle variabilities are used to assess coating quality. Inter-particle variability, a measure of the distribution of the coating mass on pellets, is obtained by dividing the standard deviation of the deposited coating mass to its mean. Intra-particle variability, a measure of film layer quality on a pellet, is obtained by dividing the standard deviation of the film thickness to its mean.

Researchers have used several techniques to monitor the coating process in the Wurster coater. Fluorescence and photoluminescence (Karlsson et al., 2006; Kitak et al., 2018), positron emission particle tracking (Fitzpatrick et al., 2003), and electrical capacitance tomography (Che et al., 2018) have been used to measure the residence time and the concentration of the pellets in various parts of the Wurster coater. Near infrared spectroscopy (Naidu et al., 2017), imaging techniques (Mehle et al., 2018; Šibanc et al., 2017), and Raman spectroscopy (Santos Silva et al., 2019) have been used to monitor film quality and operation stability the during coating operation.

Mathematical modeling is another tool for studying the coating process. Combined computational fluid dynamics and discrete element method (CFD-DEM) simulations have been used to predict the distribution of the pellet residence time (Böhling et al., 2019; Golshan et al., 2017; Li et al., 2015b, 2016) and find coating mass distribution using a simple spray sub-model (Hilton et al., 2013). Jiang et al. (2018) used CFD-DEM to predict residence time distribution, drop deposition, and collision velocity of a binary mixture in a Wurster bed.

CFD-DEM simulations are limited by their computational intensiveness. Parallelization is a solution to this problem. Two main approaches are shared-memory and distributed-memory parallelization. DEM is

E-mail address: h.norouzi@aut.ac.ir.

https://doi.org/10.1016/j.ijpharm.2020.119931
Received 24 March 2020; Received in revised form 20 September 2020; Accepted 26 September 2020
Available online 1 October 2020

Nomenclature

symbol	description
A_{film}	surface area of film, [m^2]
A_i	pellet area, [m^2]
B_M	Spalding mass transfer number, [-]
C_k	concentrating of solvent, [kg/m^3]
CoV_{inter}	inter-particle variability, [-]
CL_i	contact list of pellet i, [-]
Cp_f	specific heat of fluid, [J/kg.K]
Cp_i	specific heat of pellet i, [J/kg.K]
Cp_l	specific heat of droplet l, [J/kg.K]
CT	circulation time, [s]
d_l	droplet diameter, [m]
$D_{k,f}$	mass diffusivity of component k, [m^2/s]
$\overrightarrow{f}^{d}_{i,p-f}$	drag force on pellet i, [N]
$\overrightarrow{f}^{d}_{l,d-f}$	drag force on droplet l, [N]
$\overrightarrow{f}^{f-p}_{i}$	fluid-particle force, [N]
$\overrightarrow{f}^{p-p}_{ij}$	contact force, [N]
$\overrightarrow{F}$	volumetric force on fluid from dispersed phase, [N/m^3]
$\overrightarrow{g}$	gravitational acceleration, [m/s^2]
h_i	pellet-fluid heat transfer coefficient, [$W/m^2.K$]
H_M	Spalding heat transfer number, [-]
I_i	moment of inertia of pellet i, [$kg.m^2$]
k	turbulent kinetic energy, [m^2/s^2]
k_f	fluid heat conductivity, [W/m.K]
k_v	number of the pellets intersect with fluid cell
K_{coat}	inter-particle variability factor, [$s^{0.5}$]
m_i	mass of pellet i, [kg]
$m_{i,k}$	mass of solvent in pellet i, [kg]
$\dot{m}_{i,k}$	mass exchange rate of component k from pellet i, [kg/s]
m_l	mass of droplet l, [kg]
$m_{l,k}$	mass of solvent in droplet l, [kg]
$\dot{m}_{l,k}$	mass exchange rate of solvent k from droplet l, [kg/s]
$\overrightarrow{M}^{r}_{ij}$	rolling friction torque, [N.m]
$\overrightarrow{M}^{t}_{ij}$	tangential torque, [N.m]
Mw_f	molecular weight of fluid, [kg/kmol]
Mw_k	molecular weight of solvent, [kg/kmol]
$\overrightarrow{n}_{il}$	normal vector between pellet an droplet, [-]
N_p	number of pellets in a fluid cell, [-]
N_d	number of droplets in a fluid cell, [-]
Nu_i	Nusselt number for pellet i, [-]
Nu_l	Nusselt number for droplet l, [-]
Oh	Ohnesorge number, [-]
Oh_{crtic}	critical Ohnesorge number, [-]
p	fluid pressure, [Pa]
P^*_k	vapor pressure of solvent, [Pa]
Pr_f	Prandtl number, [-]
$q_{i,vap}$	heat exchanged due to vaporization in pellet i, [W]
$q_{l,vap}$	heat exchanged due to vaporization in droplet l, [W]
$q_{i,p-f}$	surface heat transfer rate with pellet i, [W]
$q_{l,d-f}$	surface heat transfer rate with droplet l, [W]
Re_{d-p}	droplet-pellet collision Reynolds number, [-]
Re_i	Reynolds number of pellet i, [-]
Re_l	Reynolds number of droplet l, [-]
Sc_f	Schmidt number, [-]
$S_{f,h}$	volumetric interphase heat exchange, [W/m^3]
Sh_i	Sherwood number of pellet i, [-]
Sh_l	Sherwood number of droplet l, [-]
$S_{Y,k}$	volumetric interphase mass exchange, [$kg/m^3.s$]
t	time, [s]
t_{coat}	coating time, [s]
T_f	fluid temperature, [K]
T_i	particle temperature, [K]
T_l	droplet temperature, [K]
$\overrightarrow{u}$	fluid velocity, [m/s]
$\overrightarrow{v}_i$	velocity of pellet i, [m/s]
$\overrightarrow{v}_l$	velocity of droplet l, [m/s]
V_{cell}	fluid cell volume, [m^3]
V_i	Volume of pellet i, [m^3]
V_n	normal relative velocity between pellet and droplet, [m/s]
$\overrightarrow{x}_i$	position of pellet i, [m]
$X_{k,eq}$	equilibrium mole fraction of solvent on droplet surface, [-]
Y_{eq}	equilibrium mass fraction of solvent on droplet surface, [-]

Greek symbols

α_f	fluid volume fraction, [-]
α_p	pellet volume fraction, [-]
β_i	pellet-fluid mass transfer coefficient, [m/s]
ε	turbulent dissipation rate, [m^2/s^3]
λ_{vap}	enthalpy of vaporization of solvent, [J/kg]
μ_{coat}	average coating mass on pellets, [kg]
μ_{CT}	average circulation time, [s]
μ_e	turbulent viscosity, [Pa.s]
μ_f	fluid viscosity, [Pa.s]
μ_l	droplet viscosity, [Pa.s]
μ_{ST}	average spray time, [s]
ρ_f	fluid density, [kg/m^3]
ρ_l	droplet density, [kg/m^3]
σ_{coat}	standard deviation of coating mass on pellets, [kg]
σ_{CT}	standard deviation of circulation time, [s]
σ_l	surface tension of droplet, [N/m]
σ_{ST}	standard deviation of spray time, [s]
τ_d	droplet time constant, [s]
$\overleftrightarrow{\tau}_f$	shear stress tensor, [Pa]
φ_i	fractional volume of pellet i residing in a cell, [-]
$\overrightarrow{\omega}_i$	rotational speed of pellet i, [rad/s]

well parallelized on the shared-memory basis and CFD on the distributed-memory basis. Therefore, a hybrid parallelization can be successful in speeding up these simulations. Norouzi et al. (2017) combined a GPU-based DEM solver and a CPU-based CFD solver (OpenFOAM®) and validated their model for bubbling fluidization and spouted beds. Forgber et al. (2020) used the GPU-based DEM, XPS, and the CPU-based CFD, AVL-Fire, and validated their model for cooling of heated particles in a fluidized bed. He et al. (2020) used HiPPS DEM on GPU and ANSYS Fulent on CPU and proposed new algorithms to enhance computational power of their code in compassion to previous codes.

Other modeling approaches such as renewal theory, developed by Mann (1983); (1979;)), and Monte-Carlo simulation have been used to predict the coating mass distribution (KuShaari et al., 2006; Shelukar et al., 2000). However, one drawback of these modeling approaches is that they need pre-measured parameters such as the distribution of the circulation time and spray time, which could be obtained experimentally or by CFD-DEM simulations. The other drawback is that these

Table 1
Main equations for the fluid phase.

Conservation Equations

$$\frac{\partial(\rho_f \alpha_f)}{\partial t} + \vec{\nabla}.(\rho_f \alpha_f \vec{u}) = 0 \quad (1)$$

$$\frac{\partial(\rho_f \alpha_f \vec{u})}{\partial t} + \vec{\nabla}.(\rho_f \alpha_f \vec{u}\vec{u}) = -\alpha_f \vec{\nabla} p - \alpha_f \vec{\nabla}.\overleftrightarrow{\tau}^{turb}_f - \vec{F} + \rho_f \varepsilon_f \vec{g} \quad (2)$$

$$\frac{\partial}{\partial t}(\alpha_f \rho_f k) + \vec{\nabla}.(\vec{u}\alpha_f \rho_f k) = \vec{\nabla}.\left(\alpha_f \frac{\mu_e}{\sigma_k}\nabla k\right) + G_f - C_D \alpha_f \rho_f \varepsilon \quad (3)$$

$$\frac{\partial}{\partial t}(\alpha_f \rho_f \varepsilon) + \vec{\nabla}.(\vec{u}\alpha_f \rho_f \varepsilon) = \vec{\nabla}.\left(\alpha_f \frac{\mu_e}{\sigma_\varepsilon}\nabla \varepsilon\right) + \frac{\varepsilon}{k}(C_1 G_f - C_2 \alpha_f \rho_f \varepsilon) \quad (4)$$

$$\frac{\partial}{\partial t}\left(\alpha_f \rho_f Cp_f T_f\right) + \vec{\nabla}.\left(\vec{u}\alpha_f \rho_f Cp_f T_f\right) = \vec{\nabla}.(\alpha_f k_f \nabla T_f) + S_{f,h} \quad (5)$$

$$\frac{\partial}{\partial t}(\alpha_f C_k) + \vec{\nabla}.(\alpha_f \vec{u} C_k) = \vec{\nabla}.(\alpha_f D_{k,f} \nabla C_k) + S_{Y,k} \quad (6)$$

Other required relations

$$\vec{F} = \frac{1}{V_{cell}}\left(\sum_{i=1}^{N_p} \vec{f}^{\,d}_{i,p-f} + \sum_{l=1}^{N_d} \vec{f}^{\,d}_{l,d-f}\right) \quad (7)$$

$$C_D = 1.0,\ C_1 = 1.44,\ C_2 = 1.92 \quad (8)$$
$$\mu_e = \mu_f + C_\mu \rho_f k^2/\varepsilon$$
$$\sigma_k = 1.0,\ \sigma_\varepsilon = 1.3$$

$$S_{f,h} = \frac{-1}{V_{cell}}\left(\sum_{l=1}^{N_d} q_{l,d-f} + \sum_{i=1}^{N_p} q_{i,p-f}\right) \quad (9)$$

$$S_{Y,k} = \frac{-1}{V_{cell}}\left(\sum_{i=1}^{N_p} \dot{m}_{i,k} + \sum_{l=1}^{N_d} \dot{m}_{l,k}\right) \quad (10)$$

models are not sensitive to spraying, heat and mass transfer conditions, and operating conditions of the coater.

We developed a comprehensive model to predict the inter-particle variability and the distributions of concentration and temperature in a Wurster coater. The model was a combination of CFD-DEM and discrete droplet method (DDM), which included the momentum, mass and energy couplings between all phases. All droplets were tracked. Droplet-pellet interactions (deposition/splashing) were also modeled. This model was implemented in parallel using a heterogeneous programming approach that uses the computational resources of CPU and GPU. The Wurster coater, Glatt® GPCG 3/5, was simulated using this code and effects of various operating conditions were investigated on the performance of the coater.

2. Model

Coating occurs in the three-phase gas–liquid-solid system in which these phases exchange momentum, heat and mass. The gas phase is hot air/nitrogen that flows through the coater and provides energy for solvent vaporization and fluidization of the pellets. The solid phase consists of pellets and the liquid phase consists of droplets.

Fig. 1 illustrates an overview of the proposed model. The model is a combination of various models at the meso- and micro-scales. Volume-averaged momentum and mass balance equations (Navier-Stokes equations), heat and species balance equations, and k-ε turbulent model constitute main model equations for the gas phase at the *meso*-scale. DEM with the soft-sphere framework describes motions of pellets at micro-scale. Pellets can exchange momentum, heat and mass with the surrounding gas.

Droplets move according to discrete droplet method. The Newton's second law of motion is applied for each individual droplet. Droplets have no interaction with each other due to their very low volume fraction (except at the region close to the atomizer nozzle). They may contact with pellets/walls and stick on the surface or splash. Solvent continuously evaporates, so a droplet may become dry. In this case, it is so light that the flowing gas carries it out of the Wurster coater. Volume and mass of the droplet are modified when evaporation occurs.

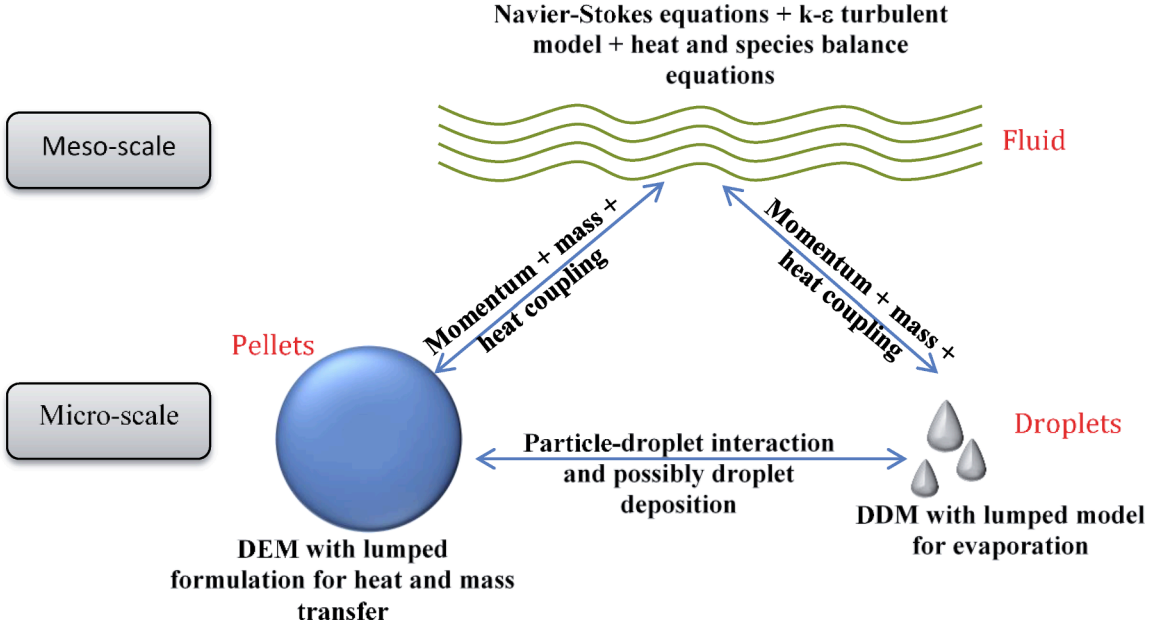

Fig. 1. Overview of the combined CFD-DEM-DDM model for the Wurster coater.

2.1. Gas phase equations

Details of the unresolved soft-sphere CFD-DEM are described elsewhere (Norouzi et al., 2016). Table 1 lists the main relations of the gas phase equations. Eqs. (1) & (2) describe the conservations of the linear momentum and the mass in the gas phase. Eqs. (3) & (4) represent the conservation equations for k-ε turbulent model and Eqs. (5) & (6), respectively, represent the the energy and species (solvent) conservations.

Terms $\vec{F}$, $S_{f,h}$, $S_{Y,k}$, $\varepsilon_f$in the conservation equations are the coupling terms between gas and pellets and between gas and droplets. In these relations, N_p is the number of the pellets in each fluid cell and N_d is the number of the droplets. All interphase exchange terms for the momentum, energy and species are sum of two terms: the transfer rate between the pellets and the gas and the transfer rate between the droplets and the gas. This indicates mutual coupling between each discrete phase and the gas phase.

In the process of solvent evaporation, a source term should be added to the right-hand side of the continuity equation to account for the evaporation. This source term is not applied here, since the mass of the vaporized solvent is almost negligible compared to the total gas flow rate. As an example, in the normal operation of the Wurster coater, the coating mass injection rate is 0.3 kg/hr and the flow rate of the hot gas may be around 150–200 kg/hr (Christensen and Bertelsen, 1997). Therefore, the total vaporized solvent into the gas phase is far less than 1% and this effect can be neglected.

2.2. Discrete element method for pellets

In DEM with the soft-sphere framework, linear and angular motions of the pellets are tracked by applying the Newton's and Euler's second laws of motion, respectively:

$$m_i \frac{d\vec{v}_i}{dt} = m_i \frac{d^2\vec{x}_i}{dt^2} = \sum_{j \in CL_i} \vec{f}_{ij}^{\,p-p} + \vec{f}_i^{\,f-p} + m_i \vec{g} \tag{11}$$

$$I_i \frac{d\vec{\omega}_i}{dt} = \sum_{j \in CL_i} \left(\vec{M}_{ij}^{\,t} + \vec{M}_{ij}^{\,r} \right) \tag{12}$$

where m_i, I_i, $\vec{v}_i$, $\vec{\omega}_i$ and $\vec{x}_i$ are the mass, the moment of inertia, the linear and the angular velocities and the center mass of the pellet i, respectively. $\vec{f}_{ij}^{\,p-p}$ is the pellet-pellet or the pellet-wall interaction force and $\vec{f}_i^{\,f-p}$ is the force exerted on the pellet from the surrounding gas. $\vec{M}_{ij}^{\,t}$ and $\vec{M}_{ij}^{\,r}$ are the tangential and rolling friction torque between a pair of pellets or a pellet and a wall. The correlations of Tsuji et al. (1992) and Di-Renzo and Di Maio (2005) provide the contact force relations in the normal and tangential directions and the correlation of Zhou et al. (1999) provides the rolling friction torque. In the above equations, the summation is performed on pellets which are in the contact list of pellets i, CL_i. Contact properties of wet pellets is modified by relating the normal restitution coefficient to surface moisture using the correlation of Crüger et al. (2015).

2.3. Coupling between pellets and gas

The equations of the gas phase are discretized over a stationary grid mesh (Eulerian approach) and time. Momentum, mass and energy couplings are performed between gas and pellets. The gas-pellet interaction force is given by (Norouzi et al., 2016):

$$\vec{f}_i^{\,f-p} = \vec{f}_{i,p-f}^{\,d} - V_i \left(\vec{\nabla} p + \vec{\nabla} . \overleftrightarrow{\tau}_f \right) \tag{13}$$

where $\vec{f}_{i,p-f}^{\,d}$ is the drag force exerted on the pellet.

Various correlations can be used for the evaluation of the drag force. Early correlations of Ergun-Wen & Yu (Ergun, 1952; Gidaspow, 1994; Wen and Yu, 1966) and Di Felice (1994) to the latest correlations by Hill et al. (2001), Benyahia et al. (2006), Beetstra et al. (2007) and Cello et al. (2010) calculate this force for spherical particles. In this study, the correlation of Beetstra et al. (2007) is used:

$$\vec{f}_{i,p-f}^{\,d} = 3\pi\mu_f \alpha_f d_i \left(\vec{u} - \vec{v}_i \right) \left\{ \left(\frac{180\alpha_p}{18\alpha_f^2} \right) + \alpha_f^2 \left(1 + 1.5\sqrt{\alpha_p} \right) + \left(\frac{0.413}{24\alpha_f^2} \right) \left(\frac{\alpha_f^{-1} + 3\alpha_p\alpha_f + 8.4Re_i^{-0.343}}{1 + 10^{3\alpha_p} Re_i^{-(1+4\varepsilon_p)/2}} \right) Re_i \right\} \tag{14}$$

where d_i is the pellet diameter, $\varepsilon_p = 1 - \varepsilon_f$ is the pellet volume fraction and $Re_i$is the Reynolds number.:

$$Re_i = \frac{\rho_f \alpha_f d_i \left| \vec{u} - \vec{v}_i \right|}{\mu_f} \tag{15}$$

The gas volume fraction in each fluid cell is calculated by:

$$\alpha_f = 1 - \frac{1}{V_{cell}} \sum_{i=1}^{k_v} \varphi_i V_i \tag{16}$$

where $k_v$is the number of the pellets fully/partially located within the fluid cell and $\varphi_i \in [0, 1]$ is the fraction of the pellet i that resides in the fluid cell. To determine φ_i, each pellet is sub-divided into 29 equal parts and this fraction is calculated based on the number of sub-divisions which resides in the cell (Norouzi, 2016; Norouzi et al., 2016).

When a droplet is deposited on a pellet surface, the droplet mass is added to the coating solution on the pellet. It is assumed that the added liquid shortly spreads on the surface and forms a liquid film with the thickness L_{film}. Suzzi et al. (2010) investigated the process of liquid spraying on a tablet. In their study, the droplet (a mixture of water and glycerin) size was 20 μm and the initial velocity was 15 m/s. They showed that film spreading took only 0.4 s to complete and a uniform film with a thickness between 20 and 30 μm was formed on the tablet.

In the operating condition of the Wurster coater, the drying time is between 3.5 and 5 s at air temperature 40 °C and between 2.5 and 4 s at air temperature 80 °C. Compared to this long drying period, we can safely assume that the film spreading occurs on the surface spontaneously. Having the total liquid volume on the surface and film thickness, the total pellet surface that is covered by the liquid film can be calculated. The conventional pellets have very low porosity and roughness (Šibanc et al., 2013). Therefore, the model neglects any permeation of the liquid into the pellet.

Fig. 2 shows a schematic of the heat and mass transfer models for the pellet. The energy balance equation for the pellet reads as:

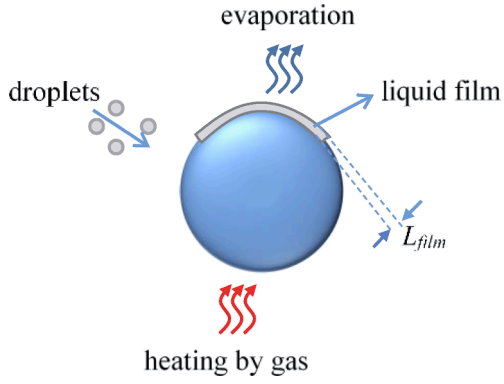

Fig. 2. Heat and mass transfer model for wet pellet.

$$m_i Cp_i \frac{dT_i}{dt} = q_{i,p-f} + q_{i,vap} = A_i h_i (T_f - T_i) + \dot{m}_{i,k} \lambda_{vap} \quad (17)$$

where $q_{i,p-f}$is the rate of the heat transfer between the gas and the pellet and $q_{i,vap}$ is the rate of the energy adsorbed by the liquid due to vaporization. The rate of vaporization,$\dot{m}_{i,k}$, is given by:

$$\frac{dm_{i,k}}{dt} = -\beta_i \rho_l A_{film} H_M \quad (18)$$

where A_{film} is the film surface area on the pellet and β_i is the mass transfer coefficient between the liquid film and the gas. The heat and mass transfer coefficients are calculated using Gunn's correlations (Gunn, 1978):

$$Nu_i = \left(7 - 10\alpha_f + 5\alpha_f^2\right)\left(1 + 0.7Re_i^{0.2}Pr_f^{1/3}\right) + \left(1.33 - 2.4\alpha_f + 1.2\alpha_f^2\right)Re_i^{0.7}Pr_f^{1/3} \quad (19)$$

$$Sh_i = \left(7 - 10\alpha_f + 5\alpha_f^2\right)\left(1 + 0.7Re_i^{0.2}Sc_f^{1/3}\right) + \left(1.33 - 2.4\alpha_f + 1.2\alpha_f^2\right)Re_i^{0.7}Sc_f^{1/3} \quad (20)$$

2.4. Modeling of spray

Experiments on the air-assisted (two fluid) atomizer show that in a distance not more than some millimeters away from the atomizer tip, the second Rayleigh-Taylor instability occurs and final droplets are formed (Aliseda et al., 2008; Varga et al., 2003). Thereafter, inter-droplet interaction is minimized due to the short time constant and low volume fraction of the droplets in the Wurster coater. The time constant of a droplet is defined as the time that takes the droplet to accelerate and reach the fluid velocity. Assuming Stokes regime, the time constant of the droplet in the fluid is given by (Crowe, 2006):

$$\tau_d = d_l^2 \rho_l / 18\mu_f \quad (21)$$

where d_l and ρ_l are the density and the diameter of the droplet. For a 30-μm droplet with the density of 1000 kg/m^3, the time constant in the air becomes 2.7 × 10^{-3} s. This low time constant shows that the droplet rapidly responds to the local change of the gas velocity and almost follows the gas phase stream line in the coater.

In two-fluid atomizers, the atomization is assisted by the cross injection of a gas jet. The gas jet velocity at the atomizer tip is between 100 and 200 m/s that is equivalent to 2 – 4 m^3/hr. This value is a very small fraction of the total volume flow rate of gas passing through the Wurster coater (almost less than 2%). Fries et al. (2011) showed that the atomizing air (in their simulation this velocity was 160 m/s) is dispersed in the surrounding fluid just 44 mm apart the atomizer tip. Therefore, atomizing jet has insignificant effect on the gas velocity in the draft tube.

Experiments and simulations on the atomization of the liquids show that the droplets are formed with the normal or lognormal size distribution and the velocity of the droplets obey the normal distribution. The average size and velocity of the droplets depends on the geometry of the atomizer, the property of the liquid and the ratio of the gas to liquid volumetric flow rate. The average size varies between 20 and 100 μm with smaller size for the bottom-mounted sprays and larger sizes for the top-mounted sprays. The spray angle (the angle of the cone that is formed by the spray) also varies between 10 and 80°and the average velocity of droplets is between 10 and 20 m/s. It was assumed that all droplets have uniform initial velocity with a pre-defined size (Aliseda et al., 2008; Heine et al., 2013; Suzzi et al., 2010; Varga et al., 2003).

Various materials are used in the formulation of the coating solution. Solvents are divided into organic and aqueous ones. Other materials such as glycerin, low molecular weight PEG, polymers, and paints present in the coating solution. In this research, aqueous solution of water and glycerin was used as the coating solution (Suzzi et al., 2010; Varga et al., 2003). Since the normal boiling point of the glycerin is 290 °C, it is expected that water vaporizes.

Following the above discussion on the spray model, the discrete droplet model was developed to describe the spray behavior. The details of the model relations are listed in Table 2. Each individual droplet is tracked by applying the Newton's second law of the motion. The relation for the translational motion is given in Eq. (22). Drag and gravity forces are considered for this motion. Miller et al. (1998) investigated 8 different models for slow, average and fast evaporation. They showed that at high evaporation rates (hydrocarbons at temperatures above 200 °C), non-equilibrium effects are significant. They also tested these models for the spraying system of coaters and showed that all 8 models similarly perform and non-equilibrium effects can be neglected. Therefore, equilibrium evaporation of droplets was used (Eqs (23) & (24)). In the present model, the Watson's relation (Viswanath and Kuloor, 1967) was used to relate enthalpy of vaporization to temperature, the Antoine's relation to relate vapor pressure to temperature, and the power rule (Cussler, 1997) to relate the diffusion coefficient to the absolute temperature.

2.5. Interaction between droplets and pellets/wall

Contact between a droplet and a surface is very complex. Yarin (2006) investigated this process and showed that the droplet may deposit and make the surface wet or bounce from it. This process depends on the factors such as the diameter, density, surface tension, viscosity and relative velocity. Mundo et al. (1995) could distinguish the conditions between droplet splashing and droplet deposition in the experiments. They stated that if the Ohnesorge number is less than the critical value given by Eq. (32), the droplet deposits on the surface otherwise it splashes. The critical Ohnesorge number is obtained from:

$$Oh_{crtic} = 57.7Re_{d-p}^{-1.25} \quad (32)$$

Table 2
Model equations for spray.

Main equations			
$m_l \frac{d\vec{v}_l}{dt} = \vec{f}_{l,d-f}^{\,d} + \vec{g}$	(22)		
$\frac{dT_l}{dt} = \frac{q_{l,d-f} + q_{l,vap}}{m_l Cp_l} = \frac{Nu_l}{3Pr_f}\left(\frac{Cp_f/Cp_l}{\tau_d}\right)(T_f - T_l) + \left(\frac{\lambda_{vap}}{Cp_l}\right)\frac{\dot{m}_{l,k}}{m_l}$	(23)		
$\frac{dm_{l,k}}{dt} = -\frac{Sh_l}{3Sc_f}\left(\frac{m_l}{\tau_d}\right)H_M$	(24)		
Sub-models			
$\vec{f}_{l,d-f}^{\,d} = 3\pi\mu_f\alpha_f d_l\left(\vec{u} - \vec{v}_l\right)\left\{(1 + 0.27Re_l)^{0.43} + \frac{0.47Re_l}{24}\left(1 - e^{(-0.04Re_l^{0.38})}\right)\right\}$	(25)*		
$Sh_l = 2 + 0.552Re_l^{0.5}Sc_f^{0.33}$	(26)*	$Nu_l = 2 + 0.552Re_l^{0.5}Pr_f^{0.33}$	(29)*
$H_M = ln(1 + B_M)$	(27)	$X_{k,eq} = X_{k,l}\gamma_k P_k^*$	(30)
$B_M = \frac{Y_{eq} - Y_f}{1 - Y_{eq}}$	(28)	$Y_{eq} = \frac{X_{k,eq}}{X_{k,eq} + (1 - X_{k,eq})(Mw_f/Mw_k)}$	(31)

* Eq. (25) is from (Cheng, 2009) and Eqs. (26) & (29) are from (Ranz and Marshall, 1952)

where the Reynolds number and other parameters are obtained from the equations bellow:

$$Re_{d-p} = \frac{\rho_l d_l V_n}{\mu_l} \tag{33}$$

$$Oh = \frac{\mu_l}{\sqrt{\rho_l \sigma_l d_l}} \tag{34}$$

$$V_n = \left| \left(\vec{v}_i - \vec{v}_l \right) \vec{n}_{il} \right| \tag{35}$$

where $\mu_l$and $\sigma_l$are the viscosity and surface tension of the droplet and $\vec{n}_{il}$is the vector that connects the pellet center to the droplet center.

To evaluate the collision conditions between droplets and pellets, consider a solution of water and glycerin. Two different droplet sizes, 30 and 100 μm, are considered. The weight percent of glycerin varies between 0 and 40. The relative velocity between pellet and droplet varies between 0.1 and 20 m/s. Fig. 3 depicts the results. Deposition occurs in the most of the operating range of interest except for the conditions that droplets are large and/or the relative velocity is high.

3. Implementation details

The details of implementation of the CFD-DEM model are given in (Norouzi et al., 2017). A brief description is given here followed by the implementation details of the new parts. The solver is broken down into three main parts: DEM and DDM solvers for pellets and droplets; CFD solver for the momentum, mass, heat and species balance equations of the gas phase; and coupling calculations for phase coupling between the pellets and the gas and between the droplets and the gas (see Fig. 4).

3.1. Implementation of the DEM and DDM solvers

The calculations related to the DEM equations are performed on GPU using CUDA platform. This massively parallel architecture allows performing millions of calculations in parallel on the shared-memory basis. The details of the implementation are presented elsewhere (Norouzi et al., 2017). The grid-based, the parallel algorithm of Mazhar et al. (2011) is used for particle–particle contact search. To represent walls in the DEM simulation, triangulation of the wall surface is done to decompose the surface into simple triangles. The contact detection between these triangles and the pellets is performed by barycentric method described elsewhere (Norouzi et al., 2016).

The DDM calculations are performed on GPU as well. Depending on the spray rate and the droplet size, it is required to simulate between 0.5 and 10 million droplets per second. If 60 s simulation is going to be performed, between 30 and 600 million droplets should be tracked in total. GPU dedicates 160 Bytes data for each droplet and for simulating 30 million of droplets, it requires around 4.5 GB of memory. This amount of memory allocation for droplets is a waste of the computational resources on the GPU and this restricts us to smaller scale simulations.

Fortunately, the average residence time of the droplet in the Wurster coater is around 0.2 s and hence the GPU actively tracks between 0.1 and 2 million droplets at a time. If the implemented algorithm reuses the memory locations of the already deleted droplets (either deposited on a surface or left the Wurster) for newly inserted droplets, less memory will be used. Inserting a large number of new droplets in empty memory locations in parallel (to minimize the execution time) requires an efficient algorithm that is described elsewhere (Norouzi, 2016).

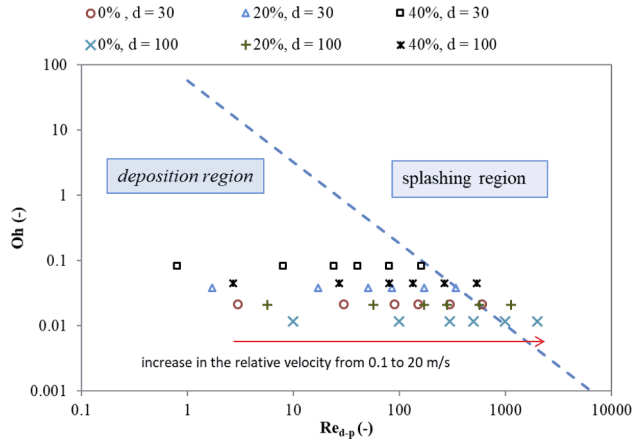

Fig. 3. Analysis of the pellet and droplets interaction with sizes 30 and 100 μm and collision velocity 0.1, 1, 3, 5, 15 and 20 m/s. The weight fraction of glycerin solution varies between 0 and 40. Properties of water-glycerin are obtained from (sheely, 1932).

3.2. Implementation of the CFD solver

The continuity, Navier-Stokes and other scalar transport equations (heat and species balances) are solved using OpenFOAM®. It is a distributed-memory, parallel code that uses space decomposition for load balancing and MPI for communication among CPU cores. A new solver, based on the PIMPLE algorithm, was developed to solve Eqs. (1) - (4) (Norouzi, 2016; Norouzi et al., 2017). After obtaining velocity field in the gas phase, the scalar transport equations (Eqs. (5) & (6)) are solved.

3.3. Implementation of coupling part

The coupling part consists of gas-pellet and gas-droplet couplings. Both were parallelized using MPI on CPU. All the required information is gathered from the CFD part (on the CPU) and the DEM & DDM parts (on the GPU). Program calculates variables such as $\vec{F}$, α_f, $S_{f,h}$, $S_{Y,k}$, $\vec{f}^{\,d}_{i,p-f}$, $q_{l,d-f}$, $q_{i,p-f}$, $\dot{m}_{i,k}$, $\dot{m}_{l,k}$ based on the relations described in the modeling section. These variables are then sent to the CFD, DEM & DDM parts for use in the calculations. More details can be found in Norouzi et al. (2017).

3.4. Simulations

The apparatus that is simulated in this study is Glatt® GPCG 3/5, Wurster 7. This is a pilot-scale Wurster coater with the total volume of 110 L. Fig. 5 depicts the dimensions of this coater. The distance between the distributor plate and the draft tube is 3 cm (10 times the pellet diameter) in the base case.

The gas distributor plate consists of 3 distinct regions in which the density and diameter of the holes are chosen in a way that a specific gas flow pattern is obtained across the plate. These regions are shown by different colors in Fig. 5. Note that the central circle belongs to the atomizer. Various gas flow patterns are used for the distributor, which are listed in Table 3.

The mesh for the CFD part is generated using a common meshing software. Cell shapes are all hex-mesh and the edge size of cells is 3 – 6 times the pellet diameter, with small cells in the bottom of the Wurster bed where the gas velocity and the pellet concentration are high and with large cells in the top part of the bed (expansion zone) where the gas velocity and the pellet concentration are low.

Pellets are spheres with the diameter 3000 μm and the density 1500 kg/m^3. Other properties are given in Table 4. All properties are based on the Cellets®, a common pellet for coating (Krok et al., 2017; Šibanc et al., 2013). The initial positions of the pellets (about 1 kg) are obtained by allowing pellets to settle under the gravity. In each simulation, the initial temperature of the pellets is equal to the gas inlet temperature (in practice, the pellets are heated up to the gas temperature before the

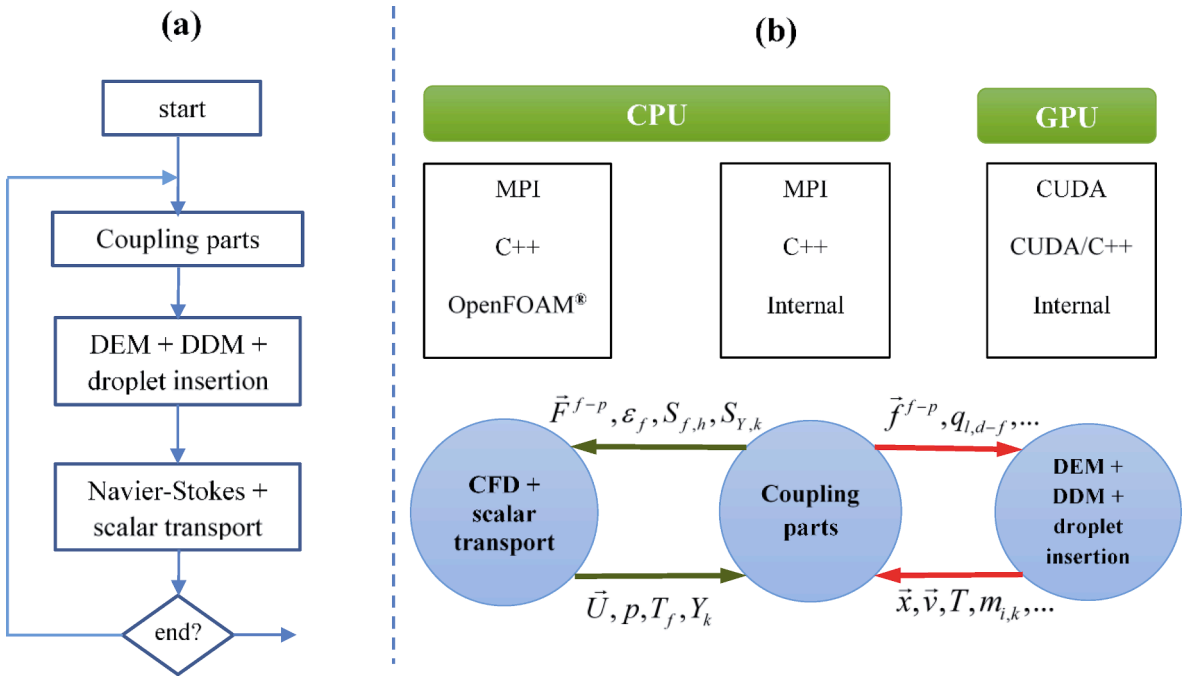

Fig. 4. Overview of the implemented solver.

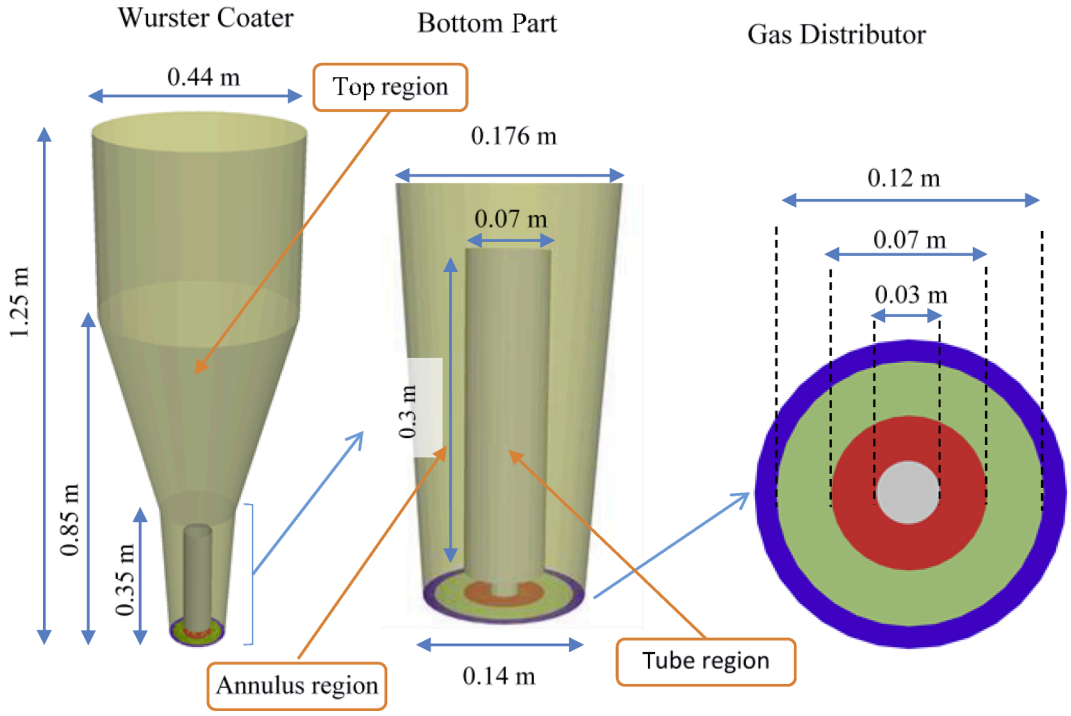

Fig. 5. Dimensions of Glatt® GPCG 3/5, Wurster 7 coater.

commence of coating operation (Christensen and Bertelsen, 1997)).

Liquid droplets are inserted through the spraying nozzle (tip of the nozzle is 4.5 cm above the distributor plate) which is located beneath the draft tube. The spraying rate is 50 mL/min. The coating solution is glycerin solution (20 wt%) at 25 °C.

The superficial gas velocity is set to the values reported in Table 3. No-slip condition is considered at the walls and fully developed condition at the outlet. At the inlet, the temperature of 40 or 80 °C and zero humidity are considered for the energy and species balance equations of the gas phase. Fully developed condition is applied at the outlet and zero gradient condition (for the energy and species balance equations) at the walls. The initial velocity and humidity of the gas and pellets are zero and the initial pellet temperature is equal to the temperature of the inlet gas. Other operating conditions and simulation settings are given in Table 4. It is a common practice to lower the Young's modulus (mostly 3 to 4 orders of magnitudes) to allow higher time steps for DEM

Table 3
Gas velocity in three regions of the distributor in various flow patterns.

	Central jet	Middle region	Perimeter region	Total flow (m^3/hr)
Flow pattern P1 [11.5]	11.5	4.1	5.5	320
Flow pattern P2 [11.5]	11.5	1.5	5.5	251
Flow pattern P3 [14.0]	14	1	1	200
Flow pattern P3 [17.0]	17	1	1	234

*velocities are in m/s

Table 4
Physical properties and simulation conditions.

Parameter	Value	Parameter	Value
Pellets (Cellets®)		Spray	
diameter (m)	0.003	rate (mL/min)	50
density (kg/m^3)	1500	velocity (m/s)	15–20
Young's modulus (MPa)	1.5	cone angle (°)	40, 80
Poisson's ratio (-)	0.23	30-μm droplet rate (1/s)	59,000,000
dynamic friction (-)	0.23	60-μm droplet rate (1/s)	7,3700,000
rolling friction (-)	0.1	100-μm droplet rate (1/s)	1,590,000
coefficient of restitution (-)	0.643	glycerin solution wt%	20
heat capacity (J/kg/K)	1380		
Simulation		Gas (Air)	
time step for particles (s)	5×10^{-6}	density and viscosity: temperature dependent	
time step for droplet (s)	5×10^{-6}		
time step for fluid (s)	1×10^{-4}	inlet temperature (°C)	40, 80
number of pellets (-)	47,200	Wurster coater	
number of cells (-)	30,000	Glatt® GPCG 3/5, Wurster 7	
simulation time (s)	90	distributor and draft tube distance (m)	0.02, 0.03

simulations. The value reported in this table is 1000 times lower than its actual value. This gives a critical time step of 1.6×10^{-4} s that is 32 times the selected time step in the simulations.

3.5. Circulation time and draft tube time

The length of time that a pellet travels in the draft tube is called draft tube time (DTT). The length of time that a pellet leaves the draft tube and re-enters it is called circulation time (CT). A program was developed in FORTRAN standard to calculate DTT and CT. Simulation results were saved on the hard disk each 0.01 s and this program read these files to calculate these quantities. In each simulation, 1000 pellets were chosen as tracers and the position of these pellets were traced for 70 s. Around 20,000 data points for DTT and CT were detected in the post processing stage of each simulation. Spray time is the other parameter that is used in the evaluation of coating process and is defined as the length of time that a pellet spends in the spray zone. If the spray sweeps the whole cross-section of the tube, the ST and the DTT would be identical.

4. Results and discussion

All simulations were performed on a desktop computer with an Intel® core™-i7 processor (4 3.6-GHz cores), 12 GB DDR3 RAM, and an NVIDIA GeForce® GTX 660Ti GPU with 2 GB DDR5 RAM. The CFD solver (using OpenFOAM® v2.4) was compiled by g++ v4.8 (Ubuntu® 14.04), and the GPU code was compiled by the CUDA® 7.0.28 compiler. The results of this program were first verified by analytical solutions and then validated using experimental results on bubbling fluidized bed and spouting bed (Norouzi et al., 2017).

4.1. Motion of pellets in the Wurster coater

Motion pattern of pellets in the Wurster coater is first studied. Experimental studies have shown that the motion pattern of pellets plays an important role on the coating mass distribution (Cheng and Turton, b, 2000a; KuShaari et al., 2006). Circulation time and draft tube time are chosen here. Entrance gas flow pattern in the Wurster coater influences the motion pattern of pellets the most (Fries et al., 2013; Heinrich et al., 2015). Three different gas flow patterns were tested in this study (see Table 3).

Fig. 6 (a) shows the distribution of the circulation time with the gas velocity pattern P1[11.5] at 40 °C. The distribution is log-normal, which has been reported in the previous experiments (Li et al., 2015b; Mann and Crosby, 1975). Most of the pellets have circulation times between 3 and 4 s. It is the length of time that the pellets stay in the expansion zone (above the draft tube) and annulus region. Based on the results, pellets stay less than 1 s in the expansion zone. Therefore, most of the circulation time is related to the residence time of the pellets in the annulus region. It was shown (Norouzi et al., 2017) that bubbling regime exists in the annulus and slugging flow in the draft tube for velocity pattern P1 [11.5]. Vertical circulations of the pellets occur in the annulus during which the pellets rise (due to drift effect of bubbles) from the distributor plate to the bed surface and then descend. This is the characteristics of bubbling regime which was previously reported (Norouzi et al., 2011). This circulating motion of pellets in the annulus region without even entering the draft tube elongates the residence time and hence causes circulation times up to 16 s. Fig. 6 (b) shows the distribution of the draft tube time of pellets with the velocity pattern P1[11.5] at 40 °C. Most of

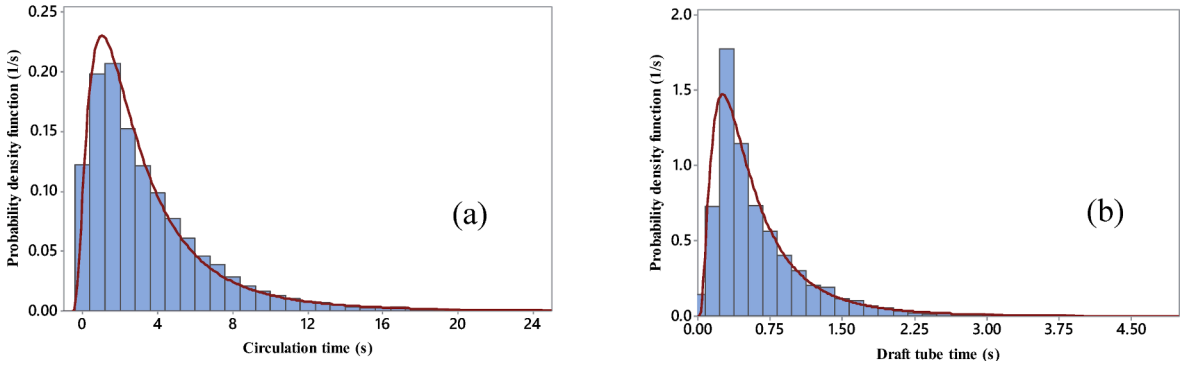

Fig. 6. (a) Circulation time and (b) draft tube time of pellets in the Wurster bed for fluid velocity pattern P1[11.5] at 40 °C.

Table 5
Mean and standard deviation of the circulation and draft tube time of pellets.

Velocity pattern [Jet velocity (m/s)]	Inlet gas temperature (°C)	Partition gap (mm)	Draft tube time (s)		Circulation time (s)		Fraction of pellets in tube (%)	Fountain height (m)
			Mean	STD	Mean	STD		
P1 [11.5]	40	30	0.62	0.5	3.46	3.28	17	0.66
P1 [11.5]	80	30	0.66	0.52	3.55	3.49	18.3	0.61
P2 [11.5]	40	30	0.67	0.53	3.81	3.8	17.8	0.67
P3 [14.0]	40	30	0.21	0.066	3.56	0.86	5.6	0.85
P3 [17.0]	40	30	0.15	0.032	3.78	0.83	3.7	1.19
P3 [14.0]	40	20	0.20	0.05	3.69	0.93	5.5	0.95
P3 [17.0]	40	20	0.15	0.031	3.83	1.1	3.6	1.22
P3 [14.0]	80	20	0.21	0.053	3.58	0.95	5.9	0.82

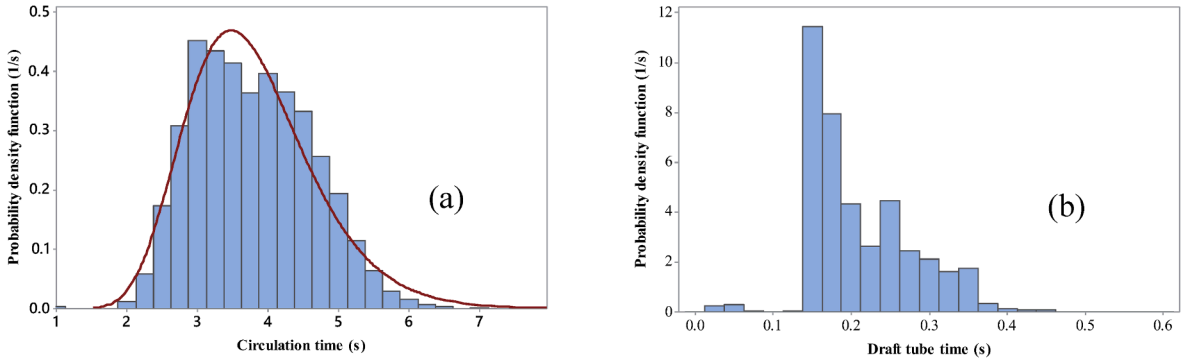

Fig. 7. (a) Circulation time and (b) draft tube time of pellets in the Wurster coater for the fluid velocity pattern P3[14] at 40 °C.

the pellets have the draft tube time of 0.4 s. But we see pellets with long draft tube time up to 2 s. This is due to the fact that the pellet-gas flow in the draft tube is slugging with high solid volume fraction and some internal circulation of pellets. In this condition, some pellets stay in the draft tube and descend near the walls and then rise in the center. This elongates the DDT and widens its distribution. Li et al. (2015a), using PEPT experiments in the Wurster bed, also observed this internal circulation (in their work they used the term "recirculation") in the draft tube region which elongates the DTT and widens the distribution of the DTT in the Wurster coater. The recirculation effect was also increased when the air velocity decreased.

Mean and standard deviation of the circulation time and draft tube time are listed in Table 5. The motion pattern of pellets with the velocity pattern P2 was similar to that with the velocity pattern P1. Hence, the detailed results are not presented here.

Fig. 7 (a) shows the distribution of the circulation time with the gas velocity pattern P3[14] at 40 °C. In comparison to the gas pattern P1 [11.5] (in Fig. 6 (a)), this distribution is narrower. It was shown (Norouzi et al., 2017) that, for velocity pattern P3[14.0], a dispersed vertical conveying of pellets exists in the draft tube and almost a suspended bed of pellets (near minimum fluidization) in the annulus. In this suspended bed, the pellets enter the draft tube layer by layer, pass through the draft tube, enter the expansion zone, and fall back on the top of this bed. This is a regular motion pattern which causes the narrow distribution of the circulation time.

Fig. 7 (b) shows the distribution of the draft tube time for the same condition. In comparison to the velocity pattern P1[11.5] (in Fig. 6 (b)), the mean and standard deviation of the draft tube time are reduced. This is attributed to the pellet flow regime (dispersed conveying) in which pellets have uniform velocity distribution in the tube and hence they reside uniformly in the tube. Looking at Table 5, an increase in the central jet velocity leads to an increase in the fountain height and a decrease in draft tube time. This is consistent with experimental observations (Li et al., 2015b).

The results in Table 5 show that the gap between the distributor plate and the draft tube also affects the CT and the DTT. When this gap is reduced from 30 mm (10 times the pellet diameter) to 20 mm (~7 times the pellet diameter), the mean and standard deviation of the circulation time are increased. Li et al. (2015b) observed the same trend when they reduced this gap from 11.5 times the particle diameter to 8.5. With this reduction, a smaller fraction of the central jet gas enters (dispersed into) the annulus region. This increases the gas velocity in the draft tube. Simulation results for P3[14.0] (results are not shown here) indicate the average gas velocity of 12.7 m/s for the gap 30 mm and the average velocity of 14.1 m/s for the gap 20 mm. Hence, the drag force acting on the pellets increases and pellets fly a higher distance in the Wurster coater and the mean circulation time is increased.

4.2. Coating operation in the Wurster coater

Although pellet motion patterns in the Wurster in terms of the circulation and draft tube time provide useful information to calculate inter-particle variability, this information is not enough. Some important questions remain unanswered:

- What is the interaction between the spray and the pellets and what if the droplet size or spray angle changes?
- What is effect of shadowing when spray does not reach the pellets in the farther layers?
- What are the temperature, mass distribution (inter-particle variability) and solvent content of pellets and how do they change with operating conditions?

Using the present CFD-DEM-DDM model, these questions can be addressed in the coating operation. The results of this model can be used to directly calculate the inter-particle variability by the following relation:

$$CoV_{inter}(t) = \frac{\sigma_{coat}(t)}{\mu_{coat}(t)} \tag{36}$$

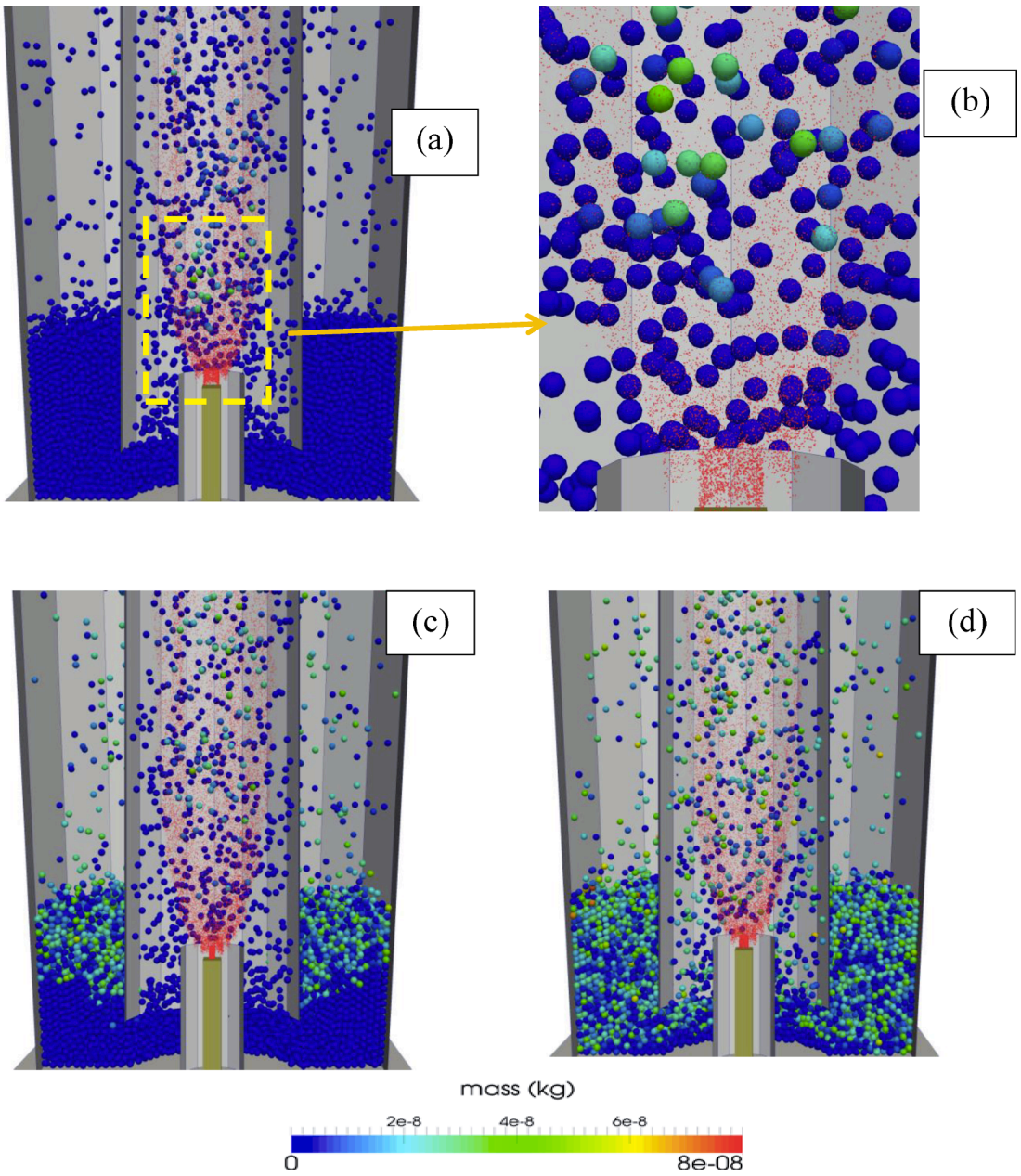

Fig. 8. The lower part of Wurster coater with the gas velocity pattern P3[14.0] at 40 °C in coating operation after (a) 0.02 s, (b) 0.02 s [enlarged], (c) 2.1 s and (d) 3.1 s. The cross section is cut in half to make inside of the bed visible. Particle are colored based on the coating mass they have received and droplets are shown with red spheres (4 times larger than their real size).

where $\mu_{coat}(t)$ and $\sigma_{coat}(t)$ are the mean and standard deviation of the coating mass deposited on the pellets at time t.

4.2.1. Inter-particle variability

Fig. 8 (a) - (d) show the half cross section of the lower part of the Wurster coater with the velocity pattern P3[14.0] at 40 °C and the droplet size 30 μm. Pellets are colored based on the coating mass that they receive. To make the droplets (red dots) visible in this view, they are rendered 4 times larger than their real size and only 10% of them are rendered. Fig. 8 (a)&(b) show 0.02 s after the start of coating operation. Pellets enter the draft tube and receive some coating mass when they rise in the draft tube. The number density of droplets decreases along the draft tube since they are deposited on the pellets. The whole cross section of the draft tube is not swept by the spray. Therefore, some pellets that enter the draft tube bypass the spray zone and do not receive any coating mass. Fig. 8 (c) and (d) show the lower part of the Wurster coater at 2.1 s and 3.1 s after start of the coating operation. Pellets that were previously in the spray zone are now collected in the annulus region and waiting to reenter the draft tube. Among these pellets, we see pellets that have not yet received any coating mass due to bypassing the spray zone which in turn widens the distribution of the coating mass on the pellets.

Fig. 9 shows the distribution of deposited coating mass on the pellets in the Wurster coater with the gas velocity pattern P1[11.5] and P3 [14.0] at 40 °C and the droplet size 30 μm. The mean coating mass increases with time and the distribution becomes broad. This distribution is log-normal and the tail is toward larger values. The same trends have been observed in the experiments of Shelukar et al. (2000) and Cheng and Turton (2000b), though differences exist between the operating conditions in the experiments and the present simulations.

Fig. 10 shows the evolution of CoV_{inter} in the Wurster coater at 40 °C. In all operating conditions, CoV_{inter} decreases with time. This decrease is sharp at first and then it becomes slow. The Wurster coater with the

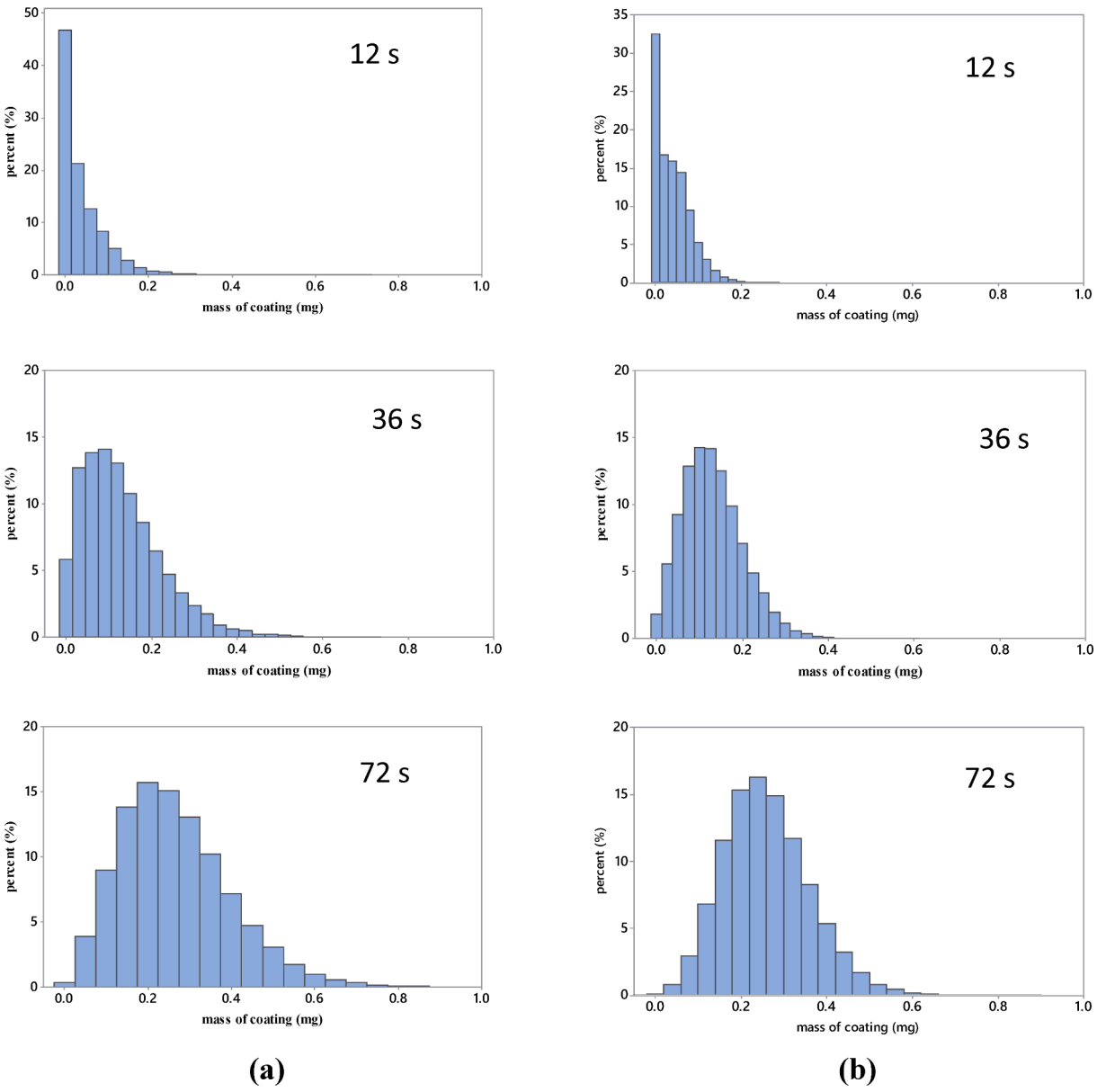

Fig. 9. Distribution of coating mass on pellets in the Wurster coater with the fluid velocity patterns (a) P1[11.5] and (b) P3[14.0] at 40 °C and the droplet size 30 μm.

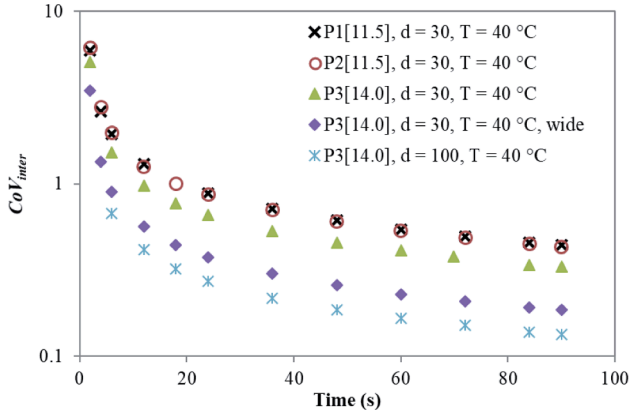

Fig. 10. Variation of inter-particle variability in the Wurster coater at various operating conditions. Droplet size in the legend is shown by letter d and its unit is μm.

velocity patterns P1 and P2 has the highest CoV_{inter}. This can associate with wide circulation and spray time (which is directly related to draft tube time) of pellets at these conditions. In contrast, CoV_{inter} is low for the Wurster coater with the velocity pattern P3 that can associate with narrow distribution of the circulation and spray time at these conditions.

According to the renewal theory, the inter-particle variability is given by (Mann, 1983):

$$CoV_{inter} = \sqrt{\frac{\mu_{CT}}{t_{coat}}\left[\left(\frac{\sigma_{ST}}{\mu_{ST}}\right)^2 + \left(\frac{\sigma_{CT}}{\mu_{CT}}\right)^2\right]} \tag{37}$$

where $\mu_{CT}$and σ_{CT} are the mean and standard deviation of the circulation time, μ_{ST} and σ_{ST} are the mean and standard deviation of the spray time. Following Eq. (37), CoV_{inter} is independent of spraying conditions. However, according to results in Fig. 10, changes in the spraying conditions, such as the droplet size and the spray angle, affect inter-particle variability. This equation can be re-written into the following form:

Table 6
Inter-particle variability factors at various conditions.

Case	Velocity pattern	Temperature (°C)	droplet diameter (μm)	Partition gap (mm)	Spray region bypass fraction (%)	$K_{coat}(s^{0.5})$	R^2
1	P1 [11.5]	40	30	30	45.0	4.21	1.0
2	P1 [11.5]	80	30	30	40.1	5.19	0.998
3	P2 [11.5]	40	30	30	47.4	4.41	0.999
4	P3 [14.0]	40	30	30	41.9	3.65	0.997
5	P3 [17.0]	40	100	30	19.3	2.14	0.985
6	P3 [14.0]	40	100	20	15.1	1.46	0.998
7	P3 [17.0]	40	100	20	22.5	2.78	0.987
8	P3 [14.0]	80	30	20	44.8	3.87	0.999
9	P3 [14.0]	40	30 (wide)	30	21.3	2.49	0.995

$$CoV_{inter} = \frac{K_{coat}}{\sqrt{t_{coat}}} \tag{38}$$

This relation shows that if CoV_{inter} is plotted against $1/\sqrt{t_{coat}}$, a straight line with slope $K_{coat}$is obtained. $K_{coat}$is called inter-particle variability factor and reflects the quality of the coating condition; low values of this factor are preferable. CoV_{inter} values obtained from each simulation were plotted as a function of $1/\sqrt{t_{coat}}$and the slopes of the straight fitted lines were calculated. The results are listed in Table 6 alongside the coefficient of determination (R^2) for each curve fitting. These coefficients show that the simulation results perfectly follow Eq. (38). The flow pattern has the most pronounced effect on CoV_{inter}. The gas temperature and the draft tube gap have the least effect and the spraying conditions have moderate effect on CoV_{inter}. Increasing the temperature from 40 to 80 °C slightly worsens CoV_{inter} (higher values of K_{coat}). This is mainly attributed to the broader distributions of the circulation time and the draft tube time (and hence spray time) at 80 °C in comparison to those at 40 °C (see Table 5). Increasing the spray angle or the droplet size improves CoV_{inter}. Knowing that distributions of the CT and the DTT do not alter, this improvement associates with the sweeping area of the spray in the draft tube. As it will be discussed in the next section, an increase in the droplet size or the spraying angle increases the sweeping area of the spray and lessens the chance of skipping spray zone.

4.2.2. Spray dynamics

Fig. 11 shows the spray shape that is formed inside the draft tube due to interactions among droplets, gas and pellets (are not rendered in this image) for two spray angles 40° and 80° (referred to as wide spray). Only 10% of the droplets are rendered (6 times larger than their real size) and they are colored based on their velocity. Since the time constant of the

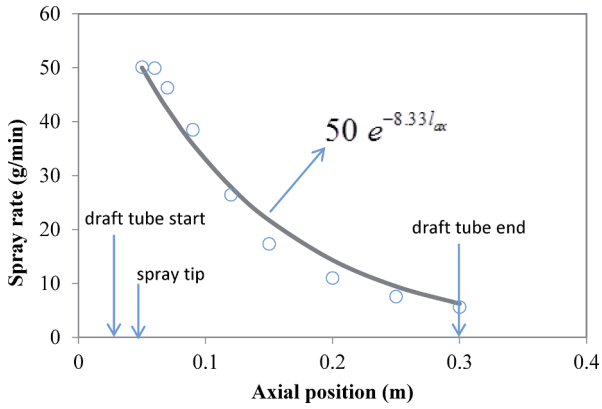

Fig. 12. Spray mass flow rate along the draft tube axis. Note that l_{ax} is axial the distance from the spray tip. Spray angle is 80°, droplet diameter is 30 μm and gas velocity pattern is P3[14.0].

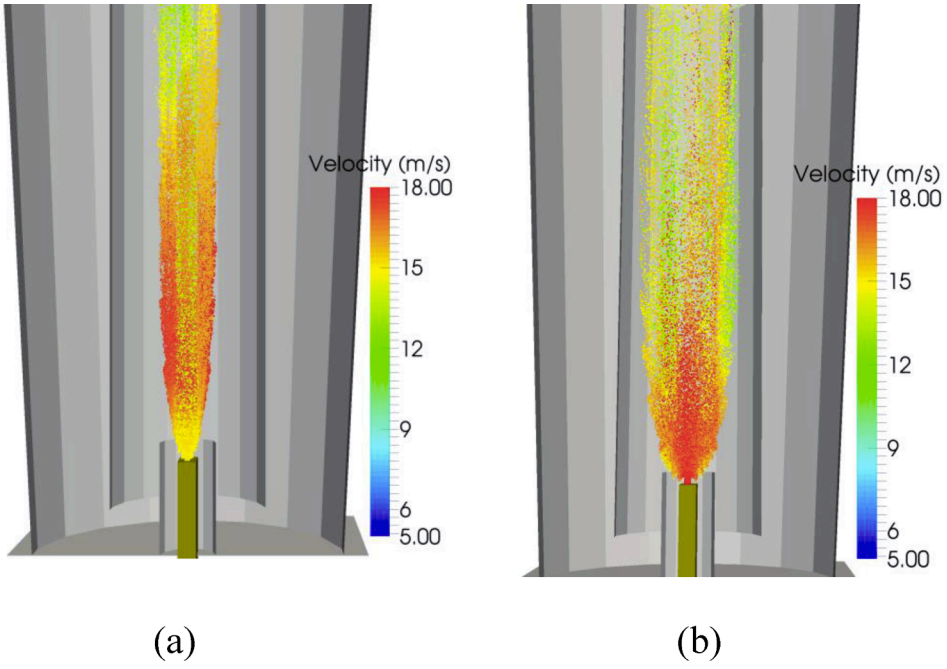

Fig. 11. Motion of droplets in the draft tube region (pellets are not rendered here). Droplets are colored based on their velocity. Droplet size is 30 μm and spray angle is (a) 40° and (b) 80° (wide). Droplets are rendered six times larger than their real size here.

droplets is very small, they rapidly reach the fluid velocity in the draft tube, so the radial motion of the droplets vanishes and they move alongside the axis of the draft tube. The spray with the wide angle sweeps a larger cross section of the draft tube and this guarantees that a larger fraction of the pellets in the draft tube receives coating solution (less probability of bypassing spraying zone). That's why we observe that the inter-particle variability factor decreases from 3.65 to 2.49 when the spray angle increases from 40° to 80° (cases 4 and 9 in Table 6). The same trend can be observed when the droplet size increases with the spraying angle of 40° (cases 4 and 6 in Table 6). The fraction of pellets that enters the tube and does not receive coating solution was calculated from simulation results and the results are listed in Table 6. As you see, these values support the conclusion on the relevance of the coating uniformity and the bypass fraction of pellets in the draft tube.

During journey of a droplet in the draft tube, its solvent evaporates, its temperature changes (not shown here) and it may interact with pellets and walls. The number density of the droplets is decreased along the draft tube. Fig. 12 shows the variation of the droplet mass flow rate along the axis of the draft tube. The spray tip is also shown on the figure where the spray mass flow is 50 g/min. Around a few millimeters above the spray tip, interaction with the pellets starts and the droplets are deposited on the pellets. The spray mass flow rate perfectly follows the decaying exponential form. The deposition rate is high at the bottom and is low near the draft tube exit. This trend also shows that around 7% of the droplets leave the draft tube and enter the expansion zone where droplet deposition is improbable. The same exponential trends were observed for other simulation cases and they are not reported here.

Fig. 13 illustrates total coating mass deposited (solvent-free basis) on pellets in the Wurster coater at various operating conditions. The dashed line in this figure shows the ideal state in which all droplets are deposited on pellets. The total coating mass deposited on the pellets is almost linear in all conditions (Guignon et al., 2003), but the slope is different. This figure shows that when the central jet velocity is 14 m/s (velocity pattern 3) and the droplet size is 30 μm, around 85 to 90% of the droplets are deposited on pellets. The best condition belongs to the wide spray (80°). When the droplet size is increased to 100 μm, only 70% of the droplets are deposited on the pellets. This associates with two factors: first, at constant mass flow rate, an increase in the droplet size reduces the number of droplets and this reduces the probability of pellet-droplet contact; and second, an increase in the droplet size may cause the droplet splashing instead of deposition (see Fig. 3). Increasing the central jet velocity reduces the coating mass deposition to 60%. When the central jet velocity increases from 14 m/s to 17 m/s, the average pellet velocity in this region increases from 3 m/s to 3.8 m/s. Droplets

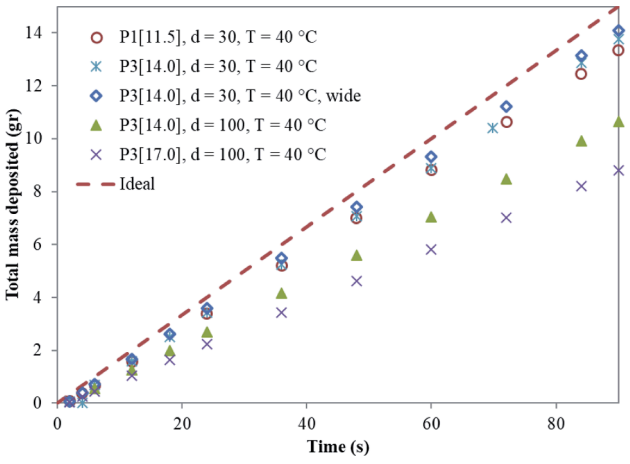

Fig. 13. Total coating mass deposited on pellets (solvent-free basis) in the Wurster coater.

rapidly reach gas velocity and their average velocity increases from 14.1 m/s to 18.1 m/s (the relative velocity between pellets and droplets, on average, increases from 11.1 m/s to 14.3 m/s). This causes more splashing of droplets in droplet-pellet contacts. In addition, the residence time of the droplets in the draft tube (where the droplet-pellet contact is the most probable) is decreased. Therefore, a larger fraction of the droplets leaves the coater without deposition on the pellets.

4.2.3. Temperature and humidity distribution

The specie balance equation (for solvent which is water here) and the energy balance equation were solved for all phases (gas, droplet and pellets) to get the distribution of the humidity and temperature over time. Although the balance equations were solved for all phases, the results of the pellet phase are only presented for the sake of brevity.

In the coating operation, the hot gas enters the coater to keep the pellets moving and vaporize the solvent on the pellets. The inlet gas velocity pattern determines the contribution of each region of the coater (draft tube, annulus and expansion zone) to the total solvent evaporation and heat exchange. Fig. 14 shows the volumetric rates of the heat exchange and evaporation in various regions of the Wurster coater (draft tube, annulus and expansion zone) for two gas velocity patterns P1 [11.5] and P3 [14.0] at 40 °C. Also, the mean fluid temperature and the mean solvent mass concentration are reported for each region. In both cases, most of the heat and mass exchanges occur in the draft tube followed by the annulus region. The exchange rates are negligible in the expansion zone. High rates of the heat and mass exchanges in the draft tube are due to the fact that most of the fresh gas that passes through the draft tube is in contact with the wet pellets and droplets. An increase in the central gas velocity reduces the rates of exchange. At higher central jet velocities, the concentration of the pellets is reduced by one-third and less wet surface is exposed to the hot gas. In the annulus region, heat exchange for the gas velocity pattern P1 is almost 3 times that for the gas velocity pattern P3. In these two conditions, number of the pellets is almost equal (similar exposed surface for heat transfer). However, the volumetric flow rate of the gas in the annulus region for the velocity patter P1 is 4.5 times larger than that for the velocity pattern P3. So, more gas has more potential for heat exchange. The same trend can be observed for the solvent evaporation in the annulus region.

Evolutions of the mean temperature and solvent mass percent of the pellets during coating operation are given in Fig. 15. In Fig. 15 (a), the mean temperature of the pellets is initially equal to the inlet gas temperature. When spraying starts, their mean temperature decreases due spray deposition and reaches a constant after about 80 s. Deposited solution on the surface of the pellet receives its heat of vaporization by the pellet itself and the surrounding gas. Therefore, pellet temperature decreases at first. In the long run, the rate of heat transfer from the gas to the surface becomes equal to the heat of vaporization and pellet temperature becomes constant.

In Fig. 15(b), the mean solvent mass percent of the pellets starts to grow at first and after reaching a maximum (except P3[14.0] at 80 °C) it decreases to a constant value. Pellets are at first dry and the solvent content of pellet increases when spraying starts. At higher gas temperature, the mean solvent concentration is lower which is obvious. In addition, gas velocity pattern has a distinct effect on the mean solvent concentration. When the velocity pattern is P1[11.5], around 200 m^3/hr of the inlet gas is in contact with 80% of the pellets in the annulus region (see Table 5) and 140 m^3/hr of the inlet gas is in contact with the rest of the pellets in the draft tube region. When velocity pattern is P3[14.0] around 45 m^3/hr of the inlet gas is in contact with around 90% of the pellets in the annulus region and 165 m^3/hr of the inlet gas with the rest of the pellets in the draft tube. This shows higher potential for mass transfer (evaporation) in the Wurster coater with the velocity pattern P1.

The above trends suggest that the coater with the velocity pattern P1 provides a more uniform condition for mass and heat transfers. So, we should expect more uniform temperature and concentration distributions on the pellets for the velocity pattern P1. In Fig. 15 (c)&(d), the

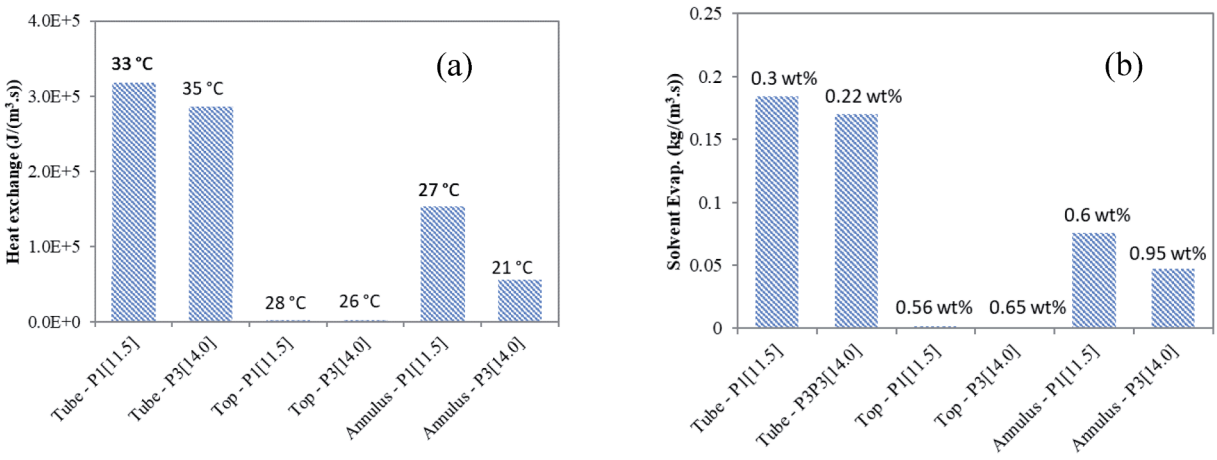

Fig. 14. Volumetric rate of (a) heat exchange and (b) solvent evaporation in various zones of the bed for two fluid velocity patterns P1[11.5] and P3[14.0] after 84 s of coating operation. The values over the bars show mean temperature and mean solvent mass percent in the gas in each region.

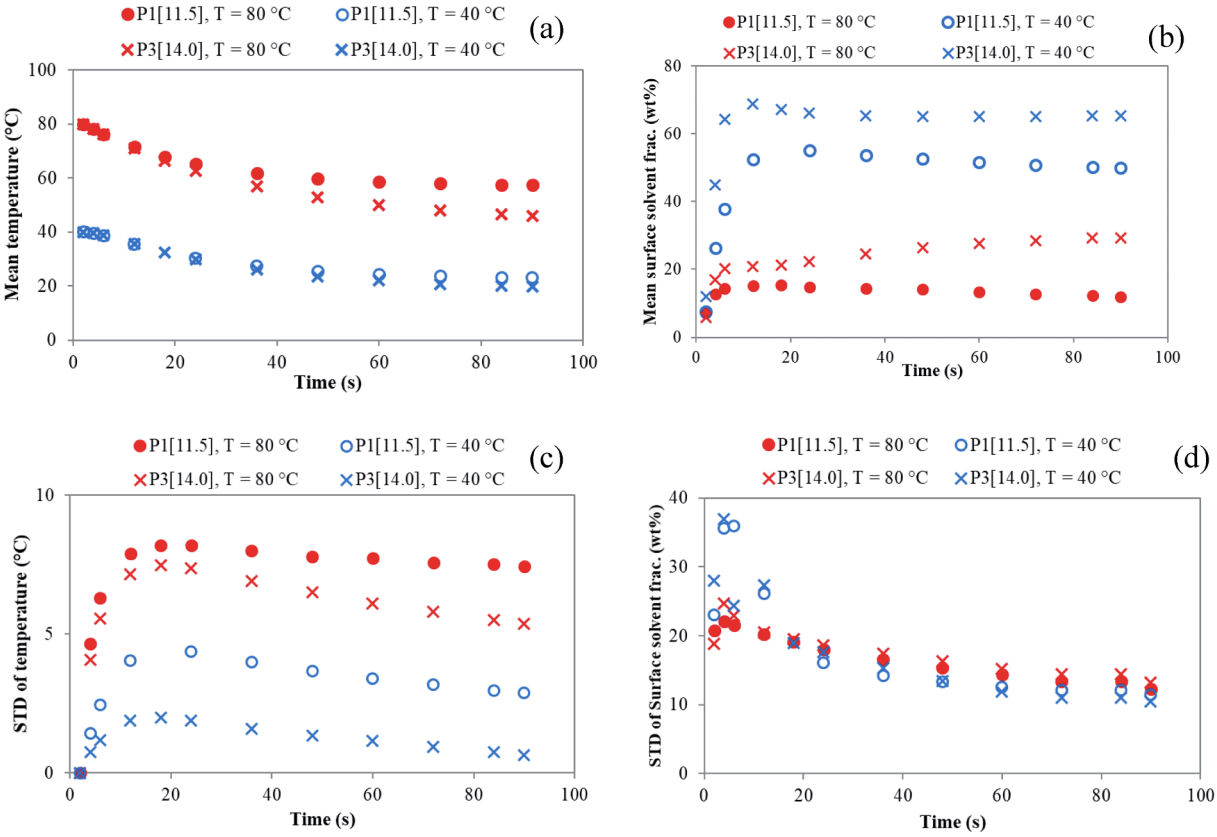

Fig. 15. Variations of (a) the mean temperature of the pellets, (b) the solvent mass percent of the pellets, (c) the standard deviation of the pellets temperature and (d) the standard deviation of solvent mass percent in the Wurster coater in the course of operation.

standard deviations of the temperature and solvent concentration do not confirm this expectation. So, we should seek for other factors that are linked to these distributions.

A closer look at what is happening in the coater reveals that variations of the solvent concentration of the pellets mainly occur due to solution deposition. Therefore, uniform solution deposition (lower values of CoV_{inter}) should cause uniform solvent concentration on the pellets. In fact, it is emphasized that both uniform deposition of coating solution and homogenous mass transfer conditions are important for uniform solvent distribution (and the first one is even more important). The correlation between CoV_{inter} and the standard deviation of the solvent concentration is shown in Fig. 16. A linear relation is observed. This clearly confirms that the solvent concentration uniformity is also linked to the distribution of deposited solution on the pellets.

4.2.4. A note on the coating condition in the Wurster

The above analysis shows that this model can reveal different aspects of the coating process in the Wurster bed. It was shown that both gas velocity pattern and spraying conditions affect CoV_{inter}. In general, more uniform circulation and spray times and larger sweeping area of the spray cause more uniform mass coating distribution. The sweeping area increases with increasing the spray angle or the droplet size. More

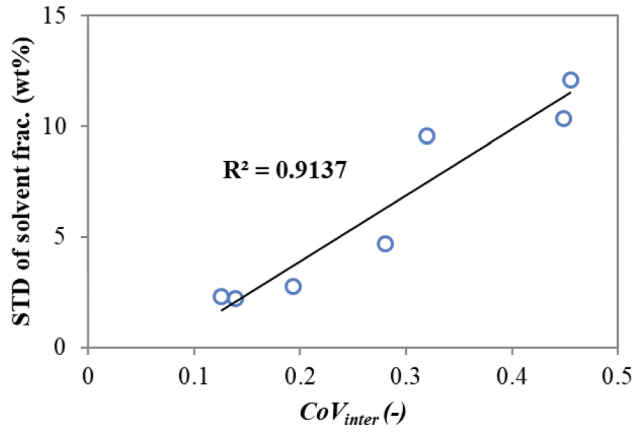

Fig. 16. Correlation between CoV_{inter} and the standard deviation of the solvent weight fraction of the pellets in the Wurster coater at 40 °C at 84 s after the start of coating.

coating mass is wasted when the droplet size increases. Hence, increasing the spray angle is a better solution. This also leads to more uniform distributions of the temperature and the concentration. Increase in the central jet velocity up to 14 m/s can also be beneficial, but further increase to 17 m/s has negative effects on the coating mass distribution and the average coating mass on pellets. Furthermore, from operational view point, low volume flow rate of the inlet gas is preferable and this is the case for P3[14.0]. Gas temperature does not significantly affect the coating mass distribution. But it influences the mean temperature and solvent content on the pellets. So, the gas temperature can be adjusted based on the operational restrictions.

5. Conclusions

Wurster coaters are commonly used for film coating of pharmaceutical pellets. The design and operation of these coaters are adjusted so that the pellets receive a uniform coating mass and they maintain a uniform temperature in the operation. Experimental techniques can be used to obtain some information about effects of the process parameters on the quality of the coated pellets. Instead, comprehensive physical models can be used to predict the distributions of the coating mass and temperature at each instant of operation. The CFD-DEM-DDM model was developed to fully simulate the coating operation. In this model, all phases are fully coupled to each other and proper sub-models are used to account for the inter-phase interactions. Model equations were implemented in parallel using a heterogeneous programming approach that uses computational resources of both CPU and GPU.

The results showed that decreasing the peripheral gas velocity, increasing the central jet velocity, and reducing the partition gap caused more uniform CT and DTT distributions while the inlet gas temperature had negligible effect. However, very high jet velocity caused a wider distribution of the CT. Though the distributions of the CT and DTT showed significant effects on the coating mass distribution, the spray dynamics and its interaction with the pellets play an equal role. Widening the spray angle while maintaining the droplet size constant caused the most uniform coating mass distribution and the highest deposition rate. In addition, heat and mass transfer conditions and deposition pattern of the coating solution influence the solvent and temperature distributions. The implemented model can be used for studying various aspects of the coating operation in the Wurster coater.

Declaration of Competing Interest

The authors declare that they have no known competing financial interests or personal relationships that could have appeared to influence the work reported in this paper.

Acknowledgement

The author would like to express their gratitude to Iran National Science Foundation (INSF) for supporting this research under grant number 96015422.

References

Aliseda, A., Hopfinger, E.J., Lasheras, J.C., Kremer, D.M., Berchielli, A., Connolly, E.K., 2008. Atomization of viscous and non-newtonian liquids by a coaxial, high-speed gas jet. Experiments and droplet size modeling. Int. J. Multiph. Flow 34, 161–175.
Ban, J., Kumar, R., Agarwal, S., Wassgren, C., 2017. Scaling inter-tablet coating variability in a horizontal rotating drum. AIChE J. 63, 3743–3755.
Beetstra, R., van der Hoef, M.A., Kuipers, J.A.M., 2007. Drag force of intermediate Reynolds number flow past mono- and bidisperse arrays of spheres. AIChE J. 53, 489–501.
Benyahia, S., Syamlal, M., O'Brien, T.J., 2006. Extension of Hill-Koch-Ladd drag correlation overall ranges of Reynolds number and solids volume fraction. Powder Technol. 162, 166–174.
Boehling, P., Toschkoff, G., Knop, K., Kleinebudde, P., Just, S., Funke, A., Rehbaum, H., Khinast, J.G., 2016. Analysis of large-scale tablet coating: Modeling, simulation and experiments. Eur. J. Pharm. Sci. 90, 14–24.
Böhling, P., Khinast, J.G., Jajcevic, D., Davies, C., Carmody, A., Doshi, P., Am Ende, M.T., Sarkar, A., 2019. Computational Fluid Dynamics-Discrete Element Method Modeling of an Industrial-Scale Wurster Coater. J. Pharm. Sci. 108, 538–550.
Cello, F., Di Renzo, A., Di Maio, F.P., 2010. A semi-empirical model for the drag force and fluid–particle interaction in polydisperse suspensions. Chem. Eng. Sci. 65, 3128–3139.
Che, H.Q., Ye, J.M., Tu, Q.Y., Yang, W.Q., Wang, H.G., 2018. Investigation of coating process in Wurster fluidised bed using electrical capacitance tomography. Chem. Eng. Res. Des. 132, 1180–1192.
Cheng, N.S., 2009. Comparison of formulas for drag coefficient and settling velocity of spherical particles. Powder Technol. 189, 395–398.
Cheng, X.X., Turton, R., 2000a. The Prediction of Variability Occurring in Fluidized Bed Coating Equipment. I. The Measurement of Particle Circulation Rates in a Bottom-Spray Fluidized Bed Coater. Pharm. Dev. Technol. 5, 311–322.
Cheng, X.X., Turton, R., 2000b. The Prediction of Variability Occurring in Fluidized Bed Coating Equipment. II. The Role of Nonuniform Particle Coverage as Particles Pass Through the Spray Zone. Pharm. Dev. Technol. 5, 323–332.
Christensen, F.N., Bertelsen, P., 1997. Qualitative Description of the Wurster-Based Fluid-Bed Coating Process. Drug Dev. Ind. Pharm. 23, 451–463.
Crowe, C.T., 2006. Multiphase Flow Handbook. Taylor & Francis.
Crüger, B., Salikov, V., Heinrich, S., Antonyuk, S., Sutkar, V.S., Deen, N.G., Kuipers, J.A.M., 2015. Coefficient of restitution for particles impacting on wet surfaces: An improved experimental approach. Particuology.
Cussler, E.L., 1997. Diffusion: Mass Transfer in Fluid Systems, 2nd ed. Cambridge University Press, New York.
Di Felice, R., 1994. The voidage function for fluid–particle interaction systems. Int. J. Multiph. Flow 20, 153–159.
Di Renzo, A., Di Maio, F.P., 2005. An improved integral non-linear model for the contact of particles in distinct element simulations. Chem. Eng. Sci. 60, 1303–1312.
Ergun, S., 1952. Fluid flow through packed columns. Chem. Eng. Prog. 48, 89–94.
Fitzpatrick, S., Ding, Y., Seiler, C., Lovegrove, C., Booth, S., Forster, R., Parker, D., Seville, J., 2003. Positron Emission Particle Tracking Studies. Pharm. Technol.
Forgber, T., Toson, P., Madlmeir, S., Kureck, H., Khinast, J.G., Jajcevic, D., 2020. Extended validation and verification of XPS/AVL-Fire™, a computational CFD-DEM software platform. Powder Technol. 361, 880–893.
Fries, L., Antonyuk, S., Heinrich, S., Dopfer, D., Palzer, S., 2013. Collision dynamics in fluidised bed granulators: A DEM-CFD study. Chem. Eng. Sci. 86, 108–123.
Fries, L., Antonyuk, S., Heinrich, S., Palzer, S., 2011. DEM–CFD modeling of a fluidized bed spray granulator. Chem. Eng. Sci. 66, 2340–2355.
Gidaspow, D., 1994. Multiphase Flow and Fluidization: Continuum and Kinetic Theory Description. Academic Press, San Diego.
Golshan, S., Zarghami, R., Mostoufi, N., 2017. Hydrodynamics of slot-rectangular spouted beds: Process intensification. Chem. Eng. Res. Des. 121, 315–328.
Guignon, B., Regalado, E., Duquenoy, A., Dumoulin, E., 2003. Helping to choose operating parameters for a coating fluid bed process. Powder Technol. 130, 193–198.
Gunn, D.J., 1978. Transfer of mass and heat to particles in fixed and fluidized beds. Int. J. Heat Mass Transf. 21, 467–476.
Hampel, N., Bück, A., Peglow, M., Tsotsas, E., 2012. Continuous pellet coating in a Wurster fluidized bed process. Chem. Eng. Sci. 86, 87–98.
He, Y., Muller, F., Hassanpour, A., Bayly, A.E., 2020. A CPU-GPU cross-platform coupled CFD-DEM approach for complex particle-fluid flows. Chem. Eng. Sci. 223, 115712.
Heine, M., Antonyuk, S., Fries, L., Niederreiter, G., Heinrich, S., Palzer, S., 2013. Modeling of the Spray Zone for Particle Wetting in a Fluidized Bed. Chem. Ing. Tech. 85, 280–289.
Heinrich, S., Dosta, M., Antonyuk, S., 2015. Multiscale Analysis of a Coating Process in a Wurster Fluidized Bed Apparatus. Advances in Chemical Engineering 46, 83–135.
Hill, R.J., Koch, D.L., Ladd, J.C., 2001. Moderate-Reynolds-numbers flows in ordered and random arrays of spheres. J. Fluid Mech. 448, 243–278.
Hilton, J.E., Ying, D.Y., Cleary, P.W., 2013. Modelling spray coating using a combined CFD–DEM and spherical harmonic formulation. Chem. Eng. Sci. 99, 141–160.

Jiang, Z., Bück, A., Tsotsas, E., 2018. CFD–DEM study of residence time, droplet deposition, and collision velocity for a binary particle mixture in a Wurster fluidized bed coater. Drying Technol. 36, 638–650.
Karlsson, S., Niklasson Björn, I., Folestad, S., Rasmuson, A., 2006. Measurement of the particle movement in the fountain region of a Wurster type bed. Powder Technol. 165, 22–29.
Kaur, S., Sivasankaran, S., Wambolt, E., Jonnalagadda, S., 2020. Determinants of zero-order release kinetics from acetaminophen-layered Suglet® pellets, Wurster-coated with plasticized Aquacoat® ECD (ethyl cellulose dispersion). Int. J. Pharm. 573, 118873.
Kitak, D., Šibanc, R., Dreu, R., 2018. Evaluation of pellet cycle times in a Wurster chamber using a photoluminescence method. Chem. Eng. Res. Des. 132, 1170–1179.
Krok, A., Vitorino, N., Zhang, J., Frade, J.R., Wu, C.-Y., 2017. Thermal properties of compacted pharmaceutical excipients. Int. J. Pharm. 534, 119–127.
KuShaari, K., Pandey, P., Song, Y., Turton, R., 2006. Monte Carlo simulations to determine coating uniformity in a Wurster fluidized bed coating process. Powder Technol. 166, 81–90.
Li, L., Rasmuson, A., Ingram, A., Johansson, M., Remmelgas, J., von Corswant, C., Folestad, S., 2015a. PEPT study of particle cycle and residence time distributions in a Wurster fluid bed. AIChE J. 61, 756–768.
Li, L., Remmelgas, J., van Wachem, B.G.M., von Corswant, C., Johansson, M., Folestad, S., Rasmuson, A., 2015b. Residence time distributions of different size particles in the spray zone of a Wurster fluid bed studied using DEM-CFD. Powder Technol. 280, 124–134.
Li, L., Remmelgas, J., Wachem, B.G.M.v., Corswant, C.v., Folestad, S., Johansson, M., Rasmuson, A., 2016. Effect of Drag Models on Residence Time Distributions of Particles in a Wurster Fluidized Bed: a DEM-CFD Study. KONA Powder and Particle Journal advpub.
Mann, U., 1983. Analysis of spouted-bed coating and granulation. 1. Batch operation. Ind Eng Chem Process Des Dev 22, 288–292.
Mann, U., Crosby, E.J., 1975. Cycle Time Distribution Measurements in Spouted Beds. The Canadian Journal of Chemical Engineering 53, 579–581.
Mann, U., Rubinovitch, M., Crosby, E.J., 1979. Characterization and analysis of continuous recycle systems. AIChE J. 25, 873–882.
Mazhar, H., Heyn, T., Negrut, D., 2011. A scalable parallel method for large collision detection problems. Multibody Sys.Dyn. 26, 37–55.
Mehle, A., Kitak, D., Podrekar, G., Likar, B., Tomaževič, D., 2018. In-line agglomeration degree estimation in fluidized bed pellet coating processes using visual imaging. Int. J. Pharm. 546, 78–85.
Miller, R.S., Harstad, K., Bellan, J., 1998. Evaluation of equilibrium and non-equilibrium evaporation models for many-droplet gas-liquid flow simulations. Int. J. Multiph. Flow 24, 1025–1055.
Mundo, C., Sommerfeld, M., Tropea, C., 1995. Droplet-wall collisions: experimental studies of the deformation and break up process. Int. J. Multiph. Flow 21, 151–173.
Naidu, V.R., Deshpande, R.S., Syed, M.R., Deoghare, P., Singh, D., Wakte, P.S., 2017. PAT-Based Control of Fluid Bed Coating Process Using NIR Spectroscopy to Monitor the Cellulose Coating on Pharmaceutical Pellets. AAPS PharmSciTech 18, 2045–2054.
Norouzi, H.R., 2016. title. University ot Tehran, University of Tehran.
Norouzi, H.R., Mostoufi, N., Mansourpour, Z., Sotudeh-Gharebagh, R., Chaouki, J., 2011. Characterization of solids mixing patterns in bubbling fluidized beds. Chem. Eng. Res. Des. 89, 817–826.
Norouzi, H.R., Zarghami, R., Mostoufi, N., 2017. New hybrid CPU-GPU solver for CFD-DEM simulation of fluidized beds. Powder Technol. 316, 233–244.
Norouzi, H.R., Zarghami, R., Sotudeh-Gharebagh, R., Mostoufi, N., 2016. Coupled CFD-DEM Modeling: Formulation. Wiley, Implementation and Application to Multiphase Flows.
Ranz, W.E., Marshall, W.R., 1952. Evaporation from drops. Chem. Eng. Prog. 48, 141–146.
Santos Silva, B., Colbert, M.-J., Santangelo, M., Bartlett, J.A., Lapointe-Garant, P.-P., Simard, J.-S., Gosselin, R., 2019. Monitoring microsphere coating processes using PAT tools in a bench scale fluid bed. Eur. J. Pharm. Sci. 135, 12–21.
Shah, N., Mehta, T., Aware, R., Shetty, V., 2017. Investigation on influence of Wurster coating process parameters for the development of delayed release minitablets of Naproxen. Drug Dev. Ind. Pharm. 43, 1989–1998.
sheely, M.L., 1932. Glycerol Viscosity Tables. Industrial & Engineering Chemistry Research 24, 1060-1064.
Shelukar, S., Ho, J., Zega, J., Roland, E., Yeh, N., Quiram, D., Nole, A., Katdare, A., Reynolds, S., 2000. Identification and characterization of factors controlling tablet coating uniformity in a Wurster coating process. Powder Technol. 110, 29–36.
Šibanc, R., Kitak, T., Govedarica, B., Srčič, S., Dreu, R., 2013. Physical properties of pharmaceutical pellets. Chem. Eng. Sci. 86, 50–60.
Šibanc, R., Luštrik, M., Dreu, R., 2017. Analysis of pellet coating uniformity using a computer scanner. Int. J. Pharm. 533, 377–382.
Suzzi, D., Radl, S., G.Khinast, J., 2010. Local analysis of the tablet coating process: Impact of operation conditions on film quality. Chemical Engineering Science 65, 5699-5715.
Teunou, E., Poncelet, D., 2002. Batch and continuous fluid bed coating – review and state of the art. J. Food Eng. 53, 325–340.
Tsuji, Y., Tanaka, T., Ishida, T., 1992. Lagrangian numerical simulation of plug flow of cohesionless particles in a horizontal pipe. Powder Technol. 71, 239–250.
Turton, R., Tardos, G.I., Ennis, B.J., 1998. Fluidized Bed Coating and Granulation. In: Yang, W.-.C. (Ed.), Fluidization, Solids Handeling, and Processing: Industrial Applications. NOYES PUBLICATIONS, Westwood, New Jersey, U.S.A.
Varga, C.M., Lasheras, J.C., Hopfinger, E.J., 2003. Initial breakup of a small diameter liquid jet by a high speed gas stream. J. Fluid Mech. 497, 405–434.
Viswanath, D.S., Kuloor, N.R., 1967. On a generalized Watson's Relation for latent heat of vaporisation. The Canadian Journal of Chemical Engineering 45, 29–31.
Wen, C.Y., Yu, Y.H., 1966. Mechanics of fluidization. Chemical Engineering Progress Symposium Series 62, 100–111.
Yarin, A.L., 2006. Drop impact dynamics : splashing, spreading, receding, bouncing. Annu. Rev. FluidMech. 38, 159–192.
Zhou, Y.C., Wright, B.D., Yang, R.Y., Xu, B.H., Yu, A.B., 1999. Rolling friction in the dynamic simulation of sandpile formation. Phys. A 269, 536–553.